

In this study, we found that the circadian expression of *c-Myc*, which is controlled by the circadian clock, affects *TFR1* gene transcription in colon cancer cells. The levels of *TFR1* mRNA and protein exhibited a 24-hour oscillation in tumor cells implanted in mice. Thus, to evaluate the rhythmic function of TFR1 and the utility for TFR1-targeting cancer therapy, we investigated how the rhythmic variation in TFR1 production influenced the pharmacologic efficacy of TFR1-targeting liposomal DDS.

Materials and Methods

Animals and cells

Seven-week-old male BALB/c mice (Charles River Japan) were housed with lights on from 7:00 a.m. to 7:00 p.m. at a room temperature of $24 \pm 1^\circ\text{C}$ and a humidity of $60 \pm 10\%$ with food and water *ad libitum*. Colon 26 cells (Cell Resource Center for Biomedical Research, Tohoku University) were maintained in RPMI 1640 supplemented 10% fetal bovine serum (FBS) at 37°C in a humidified 5% CO_2 atmosphere. A 25- μL volume with 2×10^7 viable tumor cells was inoculated into the right hind footpad of each mouse. The tumor volume was estimated according to a formula that has been described previously (7). Tissue slices of the removed tumor masses were made, and the tumor tissue was confirmed histopathologically.

Experimental design

To assess the temporal expression profile of TFR1 in tumor cells, tumor masses were removed from individual tumor-bearing mice at six different time points (9:00 a.m., 1:00 p.m., 5:00 p.m., 9:00 p.m., 1:00 a.m., and 5:00 a.m.) 7 days after the implantation of tumor cells. The levels of *TFR1* protein and mRNA were measured by Western blotting analysis and quantitative reverse transcription-PCR (RT-PCR), respectively. To investigate how the rhythmic variation in *TFR1* expression occurs in tumor cells, the influence of CLOCK/BMAL1 and c-MYC on the transcriptional activity of the *TFR1* gene was assessed using luciferase reporter constructs containing wild-type E-box or mutated E-box of the mouse *TFR1* promoter, which was based on previous reports. To elucidate the role of c-MYC in the control of the rhythmic expression of *TFR1*, endogenous c-MYC in Colon 26 cells was downregulated by small interfering RNA (siRNA). The c-MYC-downregulated cells were treated with 50% FBS for 2 hours to synchronize their circadian clock, and the mRNA levels of *TFR1* were assessed at 44, 48, 52, 56, 60, 64, and 68 hours after 50% serum treatment. In the same manner as described above, the protein levels of c-MYC and CLOCK were assessed by Western blotting analysis. To explore the temporal binding of endogenous c-MYC and CLOCK to the E-box in the mouse *TFR1* gene, chromatin immunoprecipitation analysis was performed in individual tumor masses at 9:00 a.m. and 9:00 p.m. To investigate the function of the 24-hour oscillation of TFR1 expression, time-dependent changes in Pt internalization into tumor cells were assessed using Tf-coupled liposomes encapsulating oxaliplatin (Tf-NGPE L-OHP). The cultured

Colon 26 cells were treated with 50% FBS as described above and then harvested for RNA extraction at 0, 6, 12, 18, and 24 hours after 50% FBS treatment. Nontreated Colon 26 cells harvested at the same time points were used as the control. At 6 or 18 hours after serum treatment, cells were exposed to Tf-NGPE L-OHP (L-OHP, 0.4 mg/mL) for 3 hours. The Pt content in the DNA was measured using an inductively coupled plasma mass spectrometer (ICP-MS). To explore the dosing time-dependent difference in the internalization of Pt into tumor cells *in vivo*, tumor-bearing mice were injected with a single dose of Tf-NGPE L-OHP at 9:00 a.m. or 9:00 p.m. Plasma and tumor DNA samples were collected only once from individual mice at 1, 3, and 6 hours after injection. The plasma concentration of Pt and its content in tumor DNA were measured as described above. Then, tumor volumes were measured throughout the duration of the experiment.

RT-PCR analysis

Total RNA was extracted using RNeasy (TaKaRa). The cDNAs of mouse *TFR1* (NM011638), *TFR2* (NM015799), *c-Myc* (NM010849), and β -*actin* (NM007393) were synthesized using PrimeScript Reverse Transcriptase (TaKaRa), and the synthesized cDNAs were amplified using GoTaq Green Master Mix (Promega). The PCR products were run on 2% agarose gels. After staining with ethidium bromide, the gel was photographed using Polaroid-type film. The density of each band was analyzed using NIH image software on a Macintosh computer. To evaluate the quantitative reliability of RT-PCR, kinetic analysis of the amplified products was performed to ensure that signals were derived only from the exponential phase of amplification, as previously described (7, 17). We evaluated the validity of our semiquantitative PCR methods using real-time PCR. cDNA was prepared by reverse transcription of total RNA. Real-time PCR analysis was performed on diluted cDNA samples with SYBR Premix Ex Taq Perfect Real-Time (TaKaRa) using a 7500 Real-time PCR system (Applied Biosystems). In addition, as confirmation of RNA extraction from each tumor cell sample, the expression level of *Vegf* mRNA was measured (Supplementary Data S1).

Western blotting analysis

Nuclear or cytoplasmic proteins in tumor masses were extracted using NE-PER Nuclear and Cytoplasmic Extraction Reagents (Pierce Biotechnology). The protein concentrations were determined using a BCA Protein Assay kit (Pierce Biotechnology). The lysate samples were separated on 6% or 10% SDS-polyacrylamide gels and transferred to polyvinylidene difluoride membranes. The membranes were reacted with antibodies against TFR1 (Zymed Laboratories), c-MYC, CLOCK, β -actin (Santa Cruz Biotechnology), or RNA pol II (Abcam). The immunocomplexes were further reacted with horseradish peroxidase-conjugated secondary antibodies and visualized using Super Signal Chemiluminescent Substrate (Pierce Biotechnology). The membranes were photographed using Polaroid-type film, and the density of each band was analyzed using NIH image software on a Macintosh computer.

Construction of reporter and expression vectors

The 5' flanking region of mouse *TfR1* (from bp +16 to +436; +1 indicates the transcription start site) gene was amplified using Elongase Enzyme mix (Invitrogen) using DNA extracted from Colon 26 cells. PCR was performed using the forward primer 5'-AGTTGAGCTC(SacI)GGCTTGTCAGCTCAGT-TAGTAG-3' and reverse primer 5'-ATGAGATATC(EcoRV)TAAATGTCGGTTGACACTAGTAACC-3'. The PCR products were purified and ligated into a pGL4 Basic vector (*TfR1*-Luc). The sequence of the CACGTG E-box (bp +290 to +295) on *TfR1*-Luc was mutated using a QuikChange site-directed mutagenesis kit (Stratagene). Expression vectors for mouse CLOCK, BMAL1, and c-Myc were constructed using cDNAs obtained from RT-PCR derived from mouse liver RNA. All coding regions were ligated into the pcDNA3.1 (+) vector (Invitrogen), as previously described (7). Protein expression levels from each expression vector in Colon 26 were assessed by Western blotting analysis (Supplementary Data S2).

Luciferase reporter assay

Colon 26 cells were seeded at 3×10^5 cells per well in six-well culture plates (BD Biosciences). After an 18-hour culture, the cells were transfected with 100 ng per well of reporter vector and 2 μ g per well (total) of expression vector using Lipofectamine LTX reagent (Invitrogen). A 0.5-ng-per-well sample of pRL-TK vector (Promega) was also cotransfected as an internal control reporter. The total amount of DNA per well was adjusted by adding pcDNA3.1 vector (Invitrogen). At 24 hours posttransfection, cells were harvested and the cell lysate was analyzed using a dual-luciferase reporter assay system (Promega). The ratio of firefly luciferase activity to *Renilla* luciferase activity in each sample served as a measure of normalized luciferase activity.

Small interfering RNA

siRNA of the mouse *c-Myc* gene was designed using BLOCK-IT RNAi Designer (Invitrogen). The siRNA oligonucleotide sequences were as follows: siRNA control sense, 5'-UAGUGUGAGCACUGUGAUUCCUUGG-3' and antisense 5'-CCAAGGAUCACAGUCUCACACUA-3'; *c-Myc* siRNA sense 5'-UAGUCGAGGUC-AUAGUCCUGUUGG-3' and antisense 5'-CCAACAGGAACUAUGACUCCUCACUA-3'. The oligonucleotides were transfected into Colon 26 cells at a final concentration of 20 nmol/L using Lipofectamine 2000 (Invitrogen).

Chromatin immunoprecipitation assays

Tumor masses were excised and treated with 1% formaldehyde for 5 minutes at room temperature to cross-link the chromatin, and the reaction was stopped by adding glycine to a final concentration of 0.125 mol/L. Each cross-linked sample was sonicated on ice and then incubated with antibodies against c-MYC, CLOCK, rabbit-IgG, or goat-IgG (Santa Cruz Biotechnology). Chromatin/antibody complexes were extracted using a protein G agarose kit (Roche). DNA was isolated using the Wizard SV Genomic DNA Purification System (Promega) and subjected to PCR using the following primers for the c-MYC binding site (E-box) of the *TfR1* pro-

motor region, forward 5'-GTGACTCCCTGTGTCAG-3' and reverse 5'-CCGTGACACTAGTAACC-3'. For PCR analysis, PCR products were amplified for 40 or 45 cycles. PCR products were run on an agarose (3%) gel, including 0.2 μ g/mL ethidium bromide, and analyzed using the NIH image software.

Determination of L-OHP (Pt) concentration

Plasma samples were obtained by centrifugation at 3,000 rpm for 3 minutes and stored at -20°C until analysis. Tumor DNA was extracted using a Wizard Genomic DNA Purification kit (Promega). Measurements of the L-OHP (Pt) content in plasma and tumor DNA were made using ICP-MS at the Center of Advanced Instrumental Analysis, Kyushu University. ICP-MS is capable of detecting very small amounts of Pt. Plasma Pt concentration and its tumor DNA content were expressed as micrograms per milliliter and nanograms per nanogram of DNA, respectively.

Determination of the antitumor effect

Seven days after the inoculation of Colon 26 cells into mice, a single injection of Tf-NGPE L-OHP (L-OHP: 0, 7.5 mg/kg, i.v.) or vehicle (9% sucrose) was given to tumor-bearing mice at 9:00 a.m. or 9:00 p.m. This dosage of Tf-NGPE L-OHP was selected based on a preliminary study (Supplementary Data S3). In all mice, the tumor volumes were measured every 3 days throughout the duration of the experiment.

Statistical analysis

ANOVA was used for multiple comparisons, and Scheffe's test was used for comparison between two groups. A 5% level of probability was considered significant.

Results

Twenty-four-hour rhythm in the expression of TfR1 in Colon 26 tumor masses

Two subtypes of TfR have been identified: TfR1 and TfR2. In implanted Colon 26 cells, *TfR1* but not *TfR2* was detectable, although *TfR2* was expressed in mouse liver (Supplementary Data S1B). The protein and mRNA levels of TfR1 in implanted Colon 26 cells showed a significant 24-hour rhythm, with higher levels during the early dark phase ($P < 0.05$; Fig. 1A and B). The increase and decrease in mRNA levels of *TfR1* seemed to cause the rhythm of TfR1 protein in Colon 26 tumor masses.

Regulation of the 24-hour rhythm in the expression of TfR1 gene by c-MYC

Among these, c-MYC is a potent activator of *TfR1* gene transcription in mice and humans, and the transactivation effect was elicited through binding to the CACGTG E-box located in the first intron region (18, 19). In addition, CLOCK/BMAL1 heterodimers also bind cooperatively to CACGTG E-box sequences and regulate the rhythmic expression of their target genes (2). Thus, to establish the relevance of the biological clock system on the expression of *TfR1*, CLOCK Δ 19 (CLOCK protein lacking transcriptional activity) was overexpressed in Colon 26 cells. Clock mutant mice have

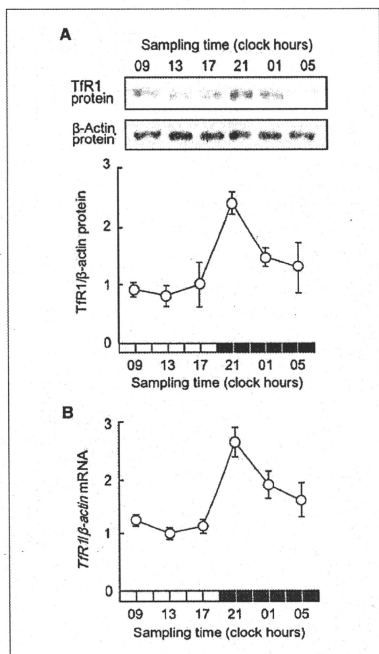


Figure 1. Twenty-four hour variation in the expression of *TTR1* in Colon 26 tumor masses. **A**, temporal expression profile of *TTR1* protein in tumor masses. The photographs show 24-h variation in *TTR1* protein in implanted Colon 26 tumor cells. Cytoplasmic proteins were measured using each of the antibodies. Bottom, relative *TTR1* protein levels. The data were normalized using β -actin as a control. Points, mean ($n = 3$, $P < 0.01$, ANOVA); bars, SEM. **B**, temporal expression profile of *TTR1* mRNA in tumor masses. The data are normalized using β -actin as a control. Points, mean ($n = 6$, $P < 0.01$, ANOVA); bars, SEM.

a point mutation in exon 19 of the *Clock* gene and exhibit low-amplitude rhythms in the expression of various genes (20). *TTR1* and *c-Myc* expression levels were low in *CLOCK* Δ 19 overexpressing Colon 26 cells (Supplementary Data S4). Next, we tested whether these transcription factors participate in regulation of the rhythmic expression of *TTR1* gene in Colon 26 cells. Cotransfection of *TTR1*-Luc with c-MYC expression constructs resulted in an 8.1-fold increase in promoter activity, whereas *CLOCK*/*BMAL1* had little effect on the transcriptional activity of the *TTR1* gene (Fig. 2B). The transactivation effect of c-MYC on *TTR1* reporters was dependent on the E-box element located from bp +290 to +295 because muta-

tion of the CACGTG sequence to AAGCTT reduced transcriptional activation by c-MYC from 8.1- to 1.5-fold.

Several compounds and high concentration serum have been shown to induce and/or synchronize circadian gene expression in cultured cells (21). Thus, to elucidate the role of c-MYC in the circadian regulation of *TTR1* expression, the temporal expression profiles of *TTR1* mRNA in c-MYC-downregulated Colon 26 cells were investigated after 50% FBS treatment. Brief exposure of control scrambled siRNA-transfected cells to 50% FBS resulted in the oscillation of *TTR1* mRNA levels with a period length of ~24 hours (Fig. 3A). On the other hand, the protein levels of c-MYC were decreased and the mRNA levels of *TTR1* failed to show a significant 24-hour oscillation after the treatment of c-Myc siRNA-transfected cells with 50% FBS (Fig. 3B and C). These results suggested that c-MYC is required for generating the time-dependent variation in *TTR1* mRNA expression.

The transcription of *c-Myc* is regulated by components of the circadian clock, and its mRNA levels in mouse liver and bones have been shown to exhibit a significant 24-hour oscillation (22). The protein levels of c-MYC in Colon 26 cells implanted in mice also showed obvious 24-hour oscillations with higher levels around the early dark phase and lower levels during the early light phase, whereas there was no obvious 24-hour variation in the protein levels of *CLOCK* in the tumor

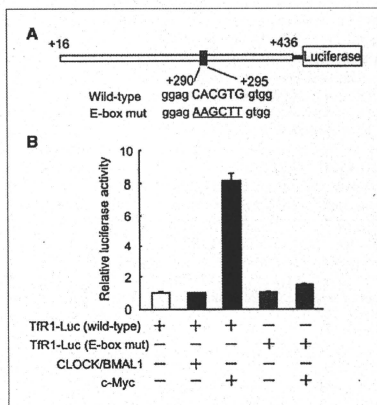


Figure 2. Influence of *CLOCK*/*BMAL1* and c-MYC on transcription of the mouse *TTR1* gene. **A**, schematic representation of the mouse *TTR1* promoter. The numbers on both sites, the distance (bp) from the transcription start site (+1) included in the luciferase reporter construction. The numbers of nucleotide residues below the box, the positions of the E-box. The underlined nucleotide residues, the mutated sequence of the E-box. **B**, wild-type or E-box-mutated *TTR1* gene reporter plasmids (*TTR1*-Luc) were cotransfected with expression constructs encoding *CLOCK*/*BMAL1* or c-MYC. Columns, mean ($n = 3$); bars, SEM.

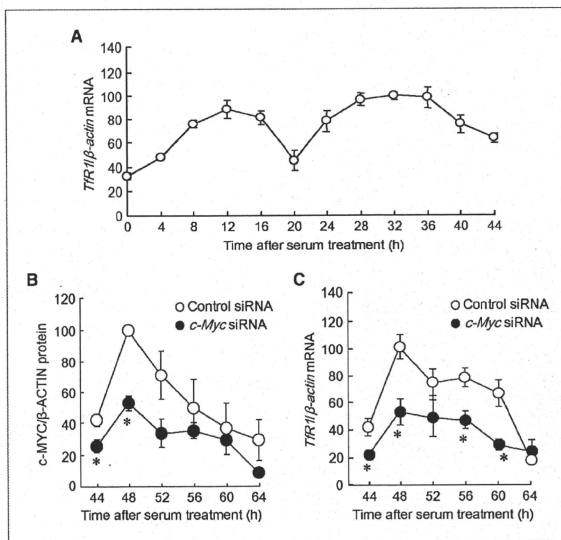


Figure 3. Influence of the downregulation of c-MYC on the rhythmic expression of *TFR1* mRNA in Colon 26 cells. **A**, temporal accumulation of *TFR1* mRNA in Colon 26 cells after 50% serum shock. The data are normalized using β -actin as a control. Points, mean ($n = 3$, $P < 0.01$, ANOVA); bars, SEM. Data are plotted relative to the 0-h value after 50% serum shock. **B**, temporal accumulation of c-MYC protein in control cells or c-Myc knockdown cells after 50% serum shock. Colon 26 cells were transfected with scrambled siRNA (control siRNA) or specific siRNAs for c-Myc (c-Myc siRNA). Crude cell extracts were measured by Western blotting analysis. The data were normalized using β -actin as a control. Points, mean ($n = 3$, control cells; $P < 0.01$, ANOVA); bars, SEM. *, $P < 0.05$, when compared with the value for the control siRNA group at the corresponding times. **C**, temporal accumulation of *TFR1* mRNA in control cells or c-Myc knockdown cells. The mRNA levels of *TFR1* were determined at the indicated time points after serum treatment. Points, mean ($n = 3$, control cells; $P < 0.01$, ANOVA); bars, SEM. *, $P < 0.05$, when compared with the value for the control siRNA group at the corresponding times.

cells (Fig. 4A). The results of chromatin immunoprecipitation analysis revealed that endogenous c-MYC in Colon 26 cells bound to the E-box element in the intron region of *TFR1* gene (Fig. 4B). Of particular note, the binding amounts of c-MYC increased at the time of day corresponding to the peak of *TFR1* mRNA expression (see Fig. 1B), suggesting that the time-dependent binding of c-MYC to the E-box in *TFR1* gene underlies its rhythmic expression. In addition, the mRNA levels of a prototypical c-MYC-regulated gene, telomerase reverse transcriptase (23), in Colon 26 cells implanted in mice also showed time-dependent variation (Supplementary Data S5).

Relationship between the rhythmic expression of *TFR1* and time dependency of Pt incorporation into tumor DNA

TF-NGPE L-OHP is a transferrin-conjugated liposome encapsulating L-OHP, a diamincyclohexane Pt antitumor agent, which forms adducts with DNA. TF-NGPE L-OHP binds to TIR, which is expressed on the plasma membrane and can

internalize Pt into the cell.³ Thus, to explore the function of internalization into the cell through transferrin in the rhythmic expression of *TFR1*, we investigated the temporal profile of *TFR1* gene expression and incorporation of Pt into tumor DNA in synchronized and desynchronized Colon 26 cells. A brief exposure of cultured Colon 26 cells to 50% FBS medium for 2 hours induced an oscillation in the expression of *TFR1* mRNA (Fig. 5A). The mRNA levels of *TFR1* peaked at 18 hours after treatment of the cells with 50% FBS. The oscillation of *TFR1* mRNA levels was also found on day 3 after serum treatment (see Fig. 3). The amount of Pt incorporated into the DNA of serum-shocked cells after treatment with TF-NGPE L-OHP increased significantly at the time point corresponding to the peak in the level of *TFR1* protein ($P < 0.05$; Fig. 5B). In contrast, in nontreated cells, neither the mRNA and protein levels of *TFR1* nor Pt incorporation showed significant time-dependent variations (Fig. 5A and B), suggesting that the oscillation in the

³ Our unpublished data.

expression of TR1 underlies the time-dependent change in Pt incorporation into tumor DNA.

Influence of dosing time on the ability of TF-NGPE L-OHP to inhibit tumor growth

The plasma Pt concentration decreased gradually after a single injection of 7.5 mg/kg TF-NGPE L-OHP (i.v.) at both dosing times, but the Pt concentration in plasma at 3 hours after TF-NGPE L-OHP injection was significantly higher in mice injected with the drug at 9:00 a.m. than at 9:00 p.m. (Fig. 6A, left). On the other hand, Pt incorporation into DNA in tumor cells at 3 and 6 hours after TF-NGPE L-OHP injection was significantly higher in mice injected with the drug at 9:00 p.m. than at 9:00 a.m. (Fig. 6A, right). We also attempted to determine the Pt contents in tumor DNA at over 6 hours after TF-NGPE L-OHP injection, but accurate assessment was difficult, probably due to L-OHP-induced apoptotic or necrotic tumor cell death.

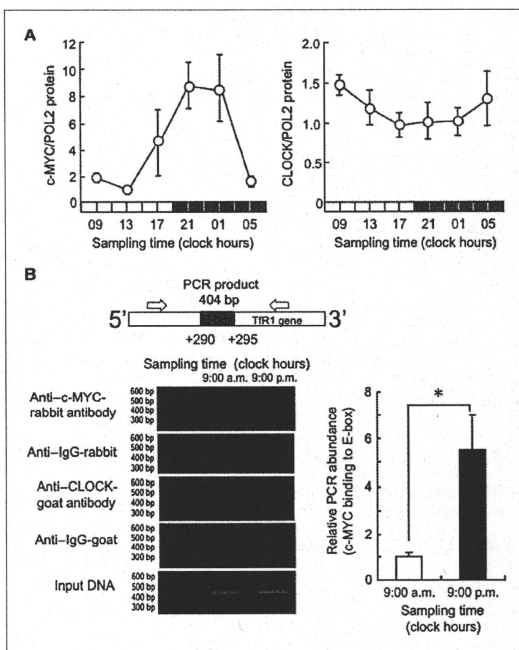
A significant antitumor effect of TF-NGPE L-OHP was observed when tumor-bearing mice were injected i.v. with a single dose of 7.5 mg/kg L-OHP (Supplementary Data S3). Thus, the dosage was set at 7.5 mg/kg to investigate whether

the antitumor effect of TF-NGPE L-OHP was altered depending on its dosing time. The growth of tumor cells was significantly suppressed by the administration of TF-NGPE L-OHP (7.5 mg/kg, i.v.). The antitumor effects were more potent in mice injected with the drug at 9:00 p.m. than in those that received it at 9:00 a.m. (Fig. 6B). Fifteen days after injection of the drug, the tumor volume in mice injected with TF-NGPE L-OHP at 9:00 p.m. was significantly smaller than that in mice injected at 9:00 a.m. ($P < 0.05$).

Discussion

TR1 is a key cell surface molecule that regulates the uptake of iron-bound transferrin (8). It has been shown that correlation exists between the number of surface TR1 and the rate of cell proliferation. TR1 expression is higher in tumor cells than in normal cells. Thus, intracellular targeting using iron-saturated Tf as a ligand for TR-mediated endocytosis has attracted attention. In this study, the protein abundance of TR1 on Colon 26 tumor cells implanted in mice showed a clear 24-hour oscillation. The rhythmic phase of TR1 protein

Figure 4. Time-dependent changes in the binding of endogenous c-MYC to the E-box element in the *TR1* gene. A, temporal expression profiles of protein levels of c-MYC and CLOCK in implanted Colon 26 tumor masses. POL2 protein was used as an internal control whose expression was constant throughout the day. The data are normalized using POL2 as a control ($P < 0.01$, ANOVA). CLOCK protein did not show an obvious variation. Points, mean ($n = 3$); bars, SEM. B, left, temporal profiles of the binding of endogenous c-MYC to the *TR1* gene in Colon 26 cells implanted in mice. Right, the quantification of temporal changes in the binding of c-MYC to the *TR1* gene in Colon 26 cells implanted in mice. The mean value of each assay at 9:00 a.m. was set at 1. Columns, mean ($n = 3$); bars, SEM. *; $P < 0.05$ for the comparison between the two groups.



paralleled that of its mRNA levels. However, the mechanisms of transcriptional rhythm of *TfR1* were unclear.

The molecular circadian clock operates at a cellular level and coordinates a wide variety of physiologic processes (24). CLOCK/BMAL1 heterodimers activate the transcription of *Per*, *Cry*, and *Dec* genes through CACGTG E-box enhancer elements (8). The results of luciferase reporter assays and chromatin immunoprecipitation experiments revealed that the CACGTG E-box located in the first intron of the mouse *TfR1* gene was unable to respond to CLOCK/BMAL1 heterodimers. In contrast, as reported previously (19), c-MYC could

bind to the E-box of the mouse *TfR1* gene and activate its transcription. The amount of endogenous c-MYC protein binding to the mouse *TfR1* gene E-box fluctuated in a time-dependent manner. The binding of c-MYC to the E-box increased at the time corresponding to the peak of *TfR1* mRNA expression, suggesting that c-MYC acts as a regulator of circadian expression of the *TfR1* gene in Colon 26 tumor cells. This hypothesis was also supported by the present findings that the amplitude of the *TfR1* mRNA rhythm in serum-shocked Colon 26 cells was decreased by the down-regulation of c-MYC. On the other hand, CLOCK protein did not bind to the *TfR1* gene E-box. This may account for the unresponsiveness of the *TfR1* gene to CLOCK/BMAL1 heterodimers. The sequence surrounding the E-box and its location had a marked influence on the transcriptional activity of CLOCK/BMAL1 (6). In fact, a CT-rich *cis*-acting element of the mouse vasopressin gene confers robust CLOCK/BMAL1 responsiveness on an adjacent E-box (25). The absence of such a CT-rich *cis*-acting element around the E-box may result in the inability of CLOCK/BMAL1 to transactivate the mouse *TfR1* gene.

Because the rhythmic phase of c-MYC protein abundance in Colon 26 cells correlated with the time dependency of its binding to the *TfR1* gene E-box, the oscillation in c-MYC protein levels may cause the 24-hour rhythm in the expression of downstream genes by rhythmic binding to their DNA response elements. In fact, *mTERT* mRNA in implanted Colon 26 tumor also showed time-dependent variation. In addition, *c-Myc* is regulated by clock genes, as indicated by previous results (26). *TfR1* and *c-Myc* expression levels were low in CLOCK Δ 19-overexpressing Colon 26 cells. Although the E-box of the *TfR1* gene did not respond to CLOCK/BMAL1, the molecular components of the circadian clock may indirectly regulate the expression of the *TfR1* gene in Colon 26 cells.

It was reported previously that L-OHP could accumulate in tumor masses following delivery using Tf-PEG liposomes (16). TfR-targeting liposomes also bind to TfR on tumor cell surfaces and are internalized into the cells by receptor-mediated endocytosis. In this study, to evaluate the function of the 24-hour oscillation in TfR1, Tf-NGPE liposomes were used as a targeting carrier for intratumoral delivery of L-OHP. This TfR-targeting liposomal DDS exhibited similar pharmacokinetic properties to Tf-PEG liposomes, and i.v. administration of L-OHP encapsulated within Tf-NGPE liposomes lead to the accumulation of a high concentration of L-OHP in tumors as much as Tf-PEG liposomes.⁴ The amount of Pt in tumor DNA after Tf-NGPE L-OHP injection increased at the times of day when TfR1 was abundant on the tumor surface in this study. This notion was also supported by *in vitro* findings that the time dependency of Tf-NGPE liposome-delivered L-OHP into tumor cells disappeared in the absence of the oscillation in TfR1 expression. These findings suggest that the oscillation in the expression of TfR1 underlies the dosing time-dependent changes in the internalization into

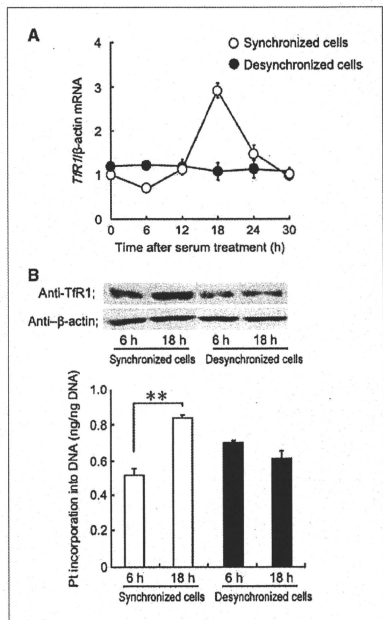
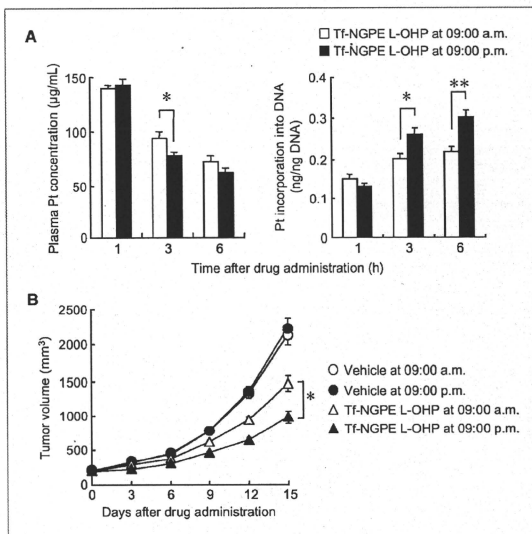


Figure 5. Influence of rhythmic changes in the expression of TfR1 on intratumoral delivery of L-OHP by Tf-NGPE liposomes. **A**, the temporal expression profile of *TfR1* mRNA in synchronized (○) or unsynchronized (●) Colon 26 cells. Cultured Colon 26 cells were synchronized (○) by exposure to 50% FBS for 2 h. Points, mean ($n = 3$, synchronized cells; $P < 0.05$, ANOVA); bars, SEM. **B**, the photographs show temporal expression of TfR1 protein in synchronized or unsynchronized Colon 26 cells. Bottom, that temporal profile of Pt incorporation into DNA in synchronized or unsynchronized Colon 26 cells. Cells were exposed to Tf-NGPE L-OHP (L-OHP: 0.4 mg/mL) for 3 h at 6 or 18 h after the serum treatment, and then the amounts of Pt incorporated into tumor DNA were measured. Columns, mean ($n = 3$); bars, SEM. *, $P < 0.05$ for the comparison between the two time points.

⁴ Our unpublished data.

Figure 6. Influence of dosing time on the ability of Tf-NGPE L-OHP to inhibit tumor growth in mice. Colon 26 tumor-bearing mice were injected i.v. with a single dose of Tf-NGPE L-OHP (L-OHP; 7.5 mg/kg) or vehicle (9% sucrose) at 9:00 a.m. or 9:00 p.m. **A**, dosing time-dependent differences in the intratumoral delivery of L-OHP by Tf-NGPE liposomes were examined. Plasma Pt concentration (left) and Pt incorporation into tumor DNA (right) were measured at the indicated times after an injection of Tf-NGPE L-OHP. Columns, mean ($n = 5$); bars, SEM; **, $P < 0.01$; *, $P < 0.05$ for comparison between the two groups. **B**, dosing time-dependent difference in the antitumor effect of Tf-NGPE L-OHP. Points, mean ($n = 8-10$); bars, SEM; *, $P < 0.05$ for comparison between the two dosing times.



the cells by receptor-mediated endocytosis. In addition, after a single injection of Tf-NGPE L-OHP, the antitumor effect of the drug varied according to its dosing time. The dosing time dependency of the antitumor effect seemed to be caused by time-dependent changes in the intratumoral delivery of L-OHP by TfR-targeting liposomes.

In the present study, it was shown that the 24-hour rhythm of TR1 expression in colon cancer cells was controlled by c-MYC, and the cyclical accumulation of TR1 caused dosing time-dependent changes in the intratumoral delivery of L-OHP by receptor-mediated endocytosis. Identification of the circadian properties of molecules that are targeted by ligand-directed DDS may aid the choice of the most appropriate time of day for their administration.

References

- Stephan FK, Zucker I. Circadian rhythms in drinking behavior and locomotor activity of rats are eliminated by hypothalamic lesions. *Proc Natl Acad Sci U S A* 1972;69:1583-6.
- Alvarez JD, Sehgal A. Circadian rhythms: finer clock control. *Nature* 2002;419:798-9.
- Gekakis N, Staknis D, Nguyen HB, et al. Role of the CLOCK protein in the mammalian circadian mechanism. *Science* 1998;280:1564-9.
- Kume K, Zylka MJ, Sriram S, et al. mCRY1 and mCRY2 are essential

Disclosure of Potential Conflicts of Interest

The authors disclose no conflicts.

Grant Support

Grants-in-Aid for Scientific Research on Priority Areas "Cancer" (S.O. 20014016) from the Ministry of Education, Culture, Sport, Science and Technology of Japan, for Scientific Research (R.S.O. 21390047), for Challenging Exploratory Research (S.O. 21659041), and for the Encouragement of Young Scientists (N.M. 20790137) from the Japan Society for the Promotion of Science.

The costs of publication of this article were defrayed in part by the payment of page charges. This article must therefore be hereby marked *advertisement* in accordance with 18 U.S.C. Section 1734 solely to indicate this fact.

Received 01/18/2010; revised 06/07/2010; accepted 06/07/2010; published OnlineFirst 07/14/2010.

components of the negative limb of the circadian clock feedback loop. *Cell* 1999;98:193-205.

- Freitner N, Damiola F, Lopez-Molina L, et al. The orphan nuclear receptor REV-ERBa controls circadian transcription within the positive limb of the mammalian circadian oscillator. *Cell* 2002; 110:251-60.
- Sato TK, Yamada RG, Ukai H, et al. Feedback repression is required for mammalian circadian clock function. *Nat Genet* 2006; 38:312-9.

7. Koyanagi S, Kuramoto Y, Nakagawa H, et al. A molecular mechanism regulating circadian expression of vascular endothelial growth factor in tumor cells. *Cancer Res* 2003;63:7277-83.
8. Daniels TR, Delgado T, Helguera G, Penichet ML. The transferrin receptor part II: targeted delivery of therapeutic agents into cancer cells. *Clin Immunol* 2006;121:159-76.
9. Sorokin LM, Morgan EH, Yeoh GC. Transformation-induced changes in transferrin and iron metabolism in myogenic cells. *Cancer Res* 1989;49:1941-7.
10. Niitsu Y, Kohgo Y, Nishisato T, et al. Transferrin receptors in human cancerous tissues. *Tohoku J Exp Med* 1987;153:239-43.
11. Calzolari A, Oliviero I, Deaglio S, et al. Transferrin receptor 2 is frequently expressed in human cancer cell lines. *Blood Cells Mol Dis* 2007;39:82-91.
12. Kawabata H, Nakamaki T, Ikonomi P, Smith RD, Germain RS, Koefler HP. Expression of transferrin receptor 2 in normal and neoplastic hematopoietic cells. *Blood* 2001;98:2714-9.
13. Röhrs S, Kutzner N, Viad A, Grunwald T, Ziegler S, Müller O. Chronological expression of Wnt target genes *Ccnd1*, *Myc*, *Cdkn1a*, *Tfrc*, *Pif1* and *Ramp3*. *Cell Biol Int* 2009;33:501-8.
14. Papanadjopoulos D, Allen TM, Gabizon A, et al. Sterically stabilized liposomes: improvements in pharmacokinetics and antitumor therapeutic efficacy. *Proc Natl Acad Sci U S A* 1991;88:11460-4.
15. Ishida O, Maruyama K, Tanahashi H, et al. Liposomes bearing polyethyleneglycol-coupled transferrin with intracellular targeting property to the solid tumors *in vivo*. *Pharm Res* 2001;18:1042-9.
16. Suzuki R, Takizawa T, Kuwata Y, et al. Effective anti-tumor activity of oxaliplatin encapsulated in transferrin-PEG-liposome. *Int J Pharm* 2008;346:143-50.
17. Ohdo S, Koyanagi S, Suyama H, Higuchi S, Aramaki H. Changing the dosing schedule minimizes the disruptive effects of interferon on clock function. *Nat Med* 2001;3:355-60.
18. Holloway K, Sade H, Romero IA, Male D. Action of transcription factors in the control of transferrin receptor expression in human brain endothelium. *J Mol Biol* 2007;365:1271-84.
19. O'Donnell KA, Yu D, Zeller KI, et al. Activation of transferrin receptor 1 by c-Myc enhances cellular proliferation and tumorigenesis. *Mol Cell Biol* 2006;26:2373-86.
20. Oishi K, Miyazaki K, Kadota K, et al. Genome-wide expression analysis of mouse liver reveals CLOCK-regulated circadian output genes. *J Biol Chem* 2003;278:41519-27.
21. Takiguchi T, Tomita M, Matsunaga N, Nakagawa H, Koyanagi S, Ohdo S. Molecular basis for rhythmic expression of CYP3A4 in serum-shocked HepG2 cells. *Pharmacogenet Genomics* 2007;17:1047-55.
22. Wittekindt NE, Hörtnagel K, Geltinger C, Polack A. Activation of c-myc promoter P1 by immunoglobulin k gene enhancers in Burkitt lymphoma: functional characterization of the intron enhancer motifs κB , E box 1 and E box 2, and of the 3' enhancer motif PU. *Nucleic Acids Res* 2000;28:800-8.
23. Reyman S, Borlak J. Transcription profiling of lung adenocarcinomas of c-myc-transgenic mice: identification of the c-myc regulatory gene network. *BMC Syst Biol* 2008;2:46.
24. Weaver Reppert SM. Coordination of circadian timing in mammals. *Nature* 2002;418:935-41.
25. Muñoz E, Brewer M, Baler R. Modulation of BMAL/CLOCK/E-Box complex activity by a CT-rich cis-acting element. *Mol Cell Endocrinol* 2006;252:74-81.
26. Fu L, Pellicano H, Liu J, Huang P, Lee C. The circadian gene *Period2* plays an important role in tumor suppression and DNA damage response *in vivo*. *Cell* 2002;111:41-50.



Development of an ultrasound-responsive and mannose-modified gene carrier for DNA vaccine therapy

Keita Un^{a,b}, Shigeru Kawakami^a, Ryo Suzuki^c, Kazuo Maruyama^c, Fumiyooshi Yamashita^a, Mitsuru Hashida^{a,d,*}

^a Department of Drug Delivery Research, Graduate School of Pharmaceutical Sciences, Kyoto University, 46-29 Yoshida-shimoadachi-cho, Sakyo-ku, Kyoto 606-8501, Japan

^b The Japan Society for the Promotion of Science (JSPS), Chiyoda-ku, Tokyo 102-8471, Japan

^c Department of Biopharmaceutics, School of Pharmaceutical Sciences, Teikyo University, 1091-1 Suwarashi, Sagami-cho, Sagami-hara, Kanagawa 229-0195, Japan

^d Institute for Integrated Cell-Material Sciences (iCeMS), Kyoto University, Yoshida-ushinomiya-cho, Sakyo-ku, Kyoto 606-8302, Japan

ARTICLE INFO

Article history:

Received 31 May 2010

Accepted 29 June 2010

Available online 24 July 2010

Keywords:

Gene transfer

Bubble lipoplexes

Ultrasound exposure

Mannose receptors

Antigen presenting cells

DNA vaccine therapy

ABSTRACT

Development of a gene delivery system to transfer the gene of interest selectively and efficiently into targeted cells is essential for achievement of sufficient therapeutic effects by gene therapy. Here, we succeeded in developing the gene transfection method using ultrasound (US)-responsive and mannose-modified gene carriers, named Man-PEG₂₀₀₀ bubble lipoplexes. Compared with the conventional lipoplex method using mannose-modified carriers, this transfection method using Man-PEG₂₀₀₀ bubble lipoplexes and US exposure enabled approximately 500–800-fold higher gene expressions in the antigen presenting cells (APCs) selectively *in vivo*. This enhanced gene expression was contributed by the improvement of delivering efficiency of nucleic acids to the targeted organs, and by the increase of introducing efficiency of nucleic acids into the cytoplasm followed by US exposure. Moreover, high antitumor effects were demonstrated by applying this method to DNA vaccine therapy using ovalbumin (OVA)-expressing plasmid DNA (pDNA). This US-responsive and cell-specific gene delivery system can be widely applied to medical treatments such as vaccine therapy and anti-inflammation therapy, which its targeted cells are APCs, and our findings may help in establishing innovative methods for *in-vivo* gene delivery to overcome the poor introducing efficiency of carriers into cytoplasm which the major obstacle associated with gene delivery by non-viral carriers.

© 2010 Elsevier Ltd. All rights reserved.

1. Introduction

In the post-genome era, the analysis of disease-related genes has rapidly advanced, and the medical application of the information obtained from gene analysis is being put into practice. In particular, the development of effective method to transfer the gene of interest selectively and efficiently into the targeted cells is essential for the gene therapy of refractory diseases, *in-vivo* functional analysis of genes and establishment of animal models for diseases. However, a suitable carrier for selective and efficient gene transfer to the targeted cells is still being developed. Although various types of viral and non-viral carriers have been developed for gene transfer, they are limited to use by viral-associated pathogenesis and low transfection efficiency, respectively. For the cell-selective gene transfer,

many investigators have focused on ligand-modified non-viral carriers such as liposomes [1–4], emulsions [5], micelles [6] and polymers [7], because of their high productivity and low toxicity. On the other hand, since the gene transfection efficiency by non-viral carriers is poor, it is difficult to obtain the effective therapeutic effects by gene therapy using non-viral carriers. Moreover, in the gene transfection using conventional ligand-modified non-viral carriers, since the carriers need to be taken up into cells via endocytosis following by interaction with targeted molecules on the cell membrane, the number of candidates which are suitable as ligands for targeted gene delivery is limited.

Some researchers have attempted to develop the transfection method using external stimulation, such as electrical energy [8], physical pressure [9] and water pressure [10], to enhance the gene transfection efficiency. Among these, gene transfection method using US exposure and microbubbles enclosing US imaging gas, called "sonoporation method", have been focused as effective drug/gene delivery systems [11–14]. In the sonoporation method, microbubbles are degraded by US exposure with optimized intensity, then cavitation energy is generated by the destruction of

* Corresponding author. Department of Drug Delivery Research, Graduate School of Pharmaceutical Sciences, Kyoto University, 46-29 Yoshida-shimoadachi-cho, Sakyo-ku, Kyoto 606-8501, Japan. Tel.: +81 75 753 4545; fax: +81 75 753 4575.

E-mail address: hashidam@pharm.kyoto-u.ac.jp (M. Hashida).

microbubbles. Consequently, the transient pores are created on the cell membrane, and large amount of nucleic acids are directly introduced into the cytoplasm through the created pores [13,15,16]. However, the in-vivo gene transfection efficiency by conventional sonoporation method administering the nucleic acids and microbubbles separately is low because of the rapid degradation of nucleic acids in the body [17], the large particle size of conventional microbubbles [15] and the different pharmacokinetic profiles of the nucleic acids and microbubbles. Moreover, to transfer the gene into the targeted cells selectively by sonoporation method in vivo, the control of in-vivo distribution of nucleic acids and microbubbles, which are separately administered, is necessary.

In our previous report [16], we have demonstrated the effective transfection by combination-use method using our mannosylated lipoplexes composed of Man-C4-*chol*:DOPE [1], and conventional Bubble liposomes (BLs) [12] with US exposure. However, this combination-use method is complicated because of the necessity for multiple injections of mannosylated lipoplexes and BLs; therefore, it is difficult to apply for medical treatments using multiple transfections. In addition, the difference of in-vivo distribution characteristics between mannosylated lipoplexes and BLs might be decreased its transfection efficacy. Therefore, it is essential to develop the US-responsive and cell-selective gene carriers constructed with ligand-modified gene carriers and microbubbles.

Taking these into considerations, we examined the gene transfection system for effective DNA vaccine therapy using physical stimulation and ligand-modification. First, we developed US-responsive and mannose-modified gene carriers, Man-PEG₂₀₀₀ bubble lipoplexes (Fig. 1), by enclosing perfluoropropane gas into mannose-conjugated PEG₂₀₀₀-DSPE-modified cationic liposomes (DSTAP: DSPC: Man-PEG₂₀₀₀-DSPE (Fig. 1))pDNA complexes. Then, we evaluated the enhanced and cell-selective gene expression in the APCs by intravenous administration of Man-PEG₂₀₀₀ bubble lipoplexes and external US exposure in mice. Finally, we examined high anti-tumor effects by applying this method to DNA vaccine therapy using OVA-expressing pDNA.

2. Materials and methods

2.1. Mice and cell lines

Female ICR mice (4–5 weeks old) and C57BL/6 mice (6–8 weeks old) were purchased from the Shizuoka Agricultural Cooperative Association for Laboratory Animals (Shizuoka, Japan). All animal experiments were carried out in accordance

with the Principles of Laboratory Animal Care as adopted and promulgated by the US National Institutes of Health and the guideline for animal experiments of Kyoto University. CD8-OVA1.3 cells, T cell hybridomas with specificity for OVA 257–264-kb, were kindly provided by Dr. C.V. Harding (Case Western Reserve University, Cleveland, OH, USA) [18]. EL4 cells (C57BL/6 T-lymphomas) and E.G7-OVA cells (the OVA-transfected clones of EL4) were purchased from American Type Culture Collection (Manassas, VA). CD8-OVA1.3 cells and EL4 cells were maintained in Dulbecco's modified Eagle's medium and E.G7-OVA cells were maintained in RPMI-1640. Both mediums were supplemented with 10% fetal bovine serum (FBS), 0.05 mM 2-mercaptoethanol, 100 IU/ml penicillin, 100 µg/ml streptomycin and 2 mM L-glutamine at 37 °C in 5% CO₂.

2.2. pDNA

pCMV-Luc and pCMV-OVA were constructed in our previous reports [19,20]. Briefly, pCMV-Luc was constructed by subcloning the HindIII/Xba I firefly luciferase cDNA fragment from pGL3-control vector (Promega, Madison, WI, USA) into the polylinker of pCDNA3 vector (Invitrogen, Carlsbad, CA, USA). pCMV-OVA was constructed by subcloning the EcoRI chicken egg albumin (ovalbumin) cDNA fragment from pAc-neo-OVA, which was kindly provided by Dr. M.J. Bevan (University of Washington, Seattle, WA, USA) into the polylinker of pVAX1. pDNA were amplified in the E. coli strain DH5α, isolated and purified using a QJAGEN Endofree Plasmid Giga Kit (QJAGEN GmbH, Hilden, Germany).

2.3. Synthesis of Man-PEG₂₀₀₀-DSPE and preparation of Man-PEG₂₀₀₀ bubble lipoplexes

Man-PEG₂₀₀₀-DSPE was synthesized in a one-step reaction by covalent binding with NH₂-PEG₂₀₀₀-DSPE (NOF Co., Tokyo, Japan) and 2-imino-2-methoxyethyl-1-thioamnoside (IME-thioamnoside). IME-thioamnoside was prepared according to the method of Lee [21]. Next, NH₂-PEG₂₀₀₀-DSPE and IME-thioamnoside were reacted, vacuum dried and dialyzed to produce Man-PEG₂₀₀₀-DSPE, and then the resultant dialysates were lyophilized. To produce the liposomes for bubble lipoplexes, DSTAP (Avanti Polar Lipids Inc., Alabaster, AL, USA), DSPC (Sigma Chemicals Inc., St. Louis, MO, USA) and Man-PEG₂₀₀₀-DSPE or NH₂-PEG₂₀₀₀-DSPE were mixed in chloroform at a molar ratio of 7:2:1. For construction of BLs, DSPC and methoxy-PEG₂₀₀₀-DSPE (NOF Co., Tokyo, Japan) were mixed in chloroform at a molar ratio of 94:6. The mixture for the construction of liposomes was dried by evaporation, vacuum desiccated and the resultant lipid film was resuspended in sterile 5% dextrose. After hydration for 30 min at 65 °C, the dispersion was sonicated for 10 min in a bath sonicator and for 3 min in a tip sonicator to produce liposomes. Then, liposomes were sterilized by passage through a 0.45 µm filter (Nihon-Millipore, Tokyo, Japan). The lipoplexes were prepared by gently mixing with equal volumes of pDNA and liposome solution at a charge ratio of 1.0:2.3 (–:–). For preparation of BLs and bubble lipoplexes, the enclosure of US imaging gas into liposomes and lipoplexes was performed according to our previous report [16]. Briefly, prepared liposomes and lipoplexes were added to 5 mL sterilized vials, filled with perfluoropropane gas (Takachiho Chemical Industries Co., Ltd., Tokyo, Japan), capped and then pressurized with 7.5 mL of perfluoropropane gas. To enclose US imaging gas into the liposomes and lipoplexes, the vial was sonicated using a bath-type sonicator (AS ONE Co., Osaka, Japan) for 5 min. The particle sizes and zeta

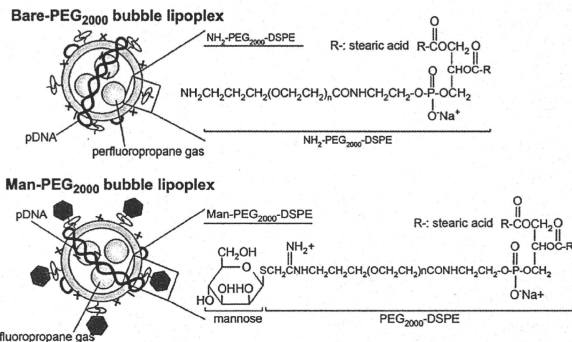


Fig. 1. Structure of Bare-PEG₂₀₀₀ bubble lipoplex containing NH₂-PEG₂₀₀₀-DSPE and Man-PEG₂₀₀₀ bubble lipoplex containing Man-PEG₂₀₀₀-DSPE used in this study.

potentials of liposomes and lipoplexes were determined by a Zetaser Nano ZS instrument (Malvern Instrument, Ltd., Worcestershire, UK).

2.4. Harvesting of mouse peritoneal macrophages

Mouse peritoneal macrophages were harvested and cultured according to our previous report [16]. Briefly, the macrophages were harvested from mice at 4 days after intraperitoneal injection of 2.9% thioglycolate medium (1 mL). The collected macrophages were washed and suspended in RPMI-1640 medium supplemented with 10% FBS, 100 IU/ml penicillin, 100 µg/ml streptomycin and 2 mM β -glutamine, and plated on culture plates. After incubation for 2 h at 37 °C in 5% CO₂, non-adherent cells were washed off with culture medium, and the macrophages were incubated for another 72 h.

2.5. In-vitro gene transfection

After the macrophages were collected and incubated for 72 h, the culture medium was replaced with Opti-MEM I containing bubble lipoplexes (5 µg pDNA). The macrophages were exposed to US (frequency, 2.062 MHz; duty, 50%; burst rate, 10 Hz; intensity 4.0 W/cm²) for 20 s using a 6 mm diameter probe placed in the well at 5 min after addition of bubble lipoplexes. In the transfection using naked pDNA and BLS, at 5 min after addition of naked pDNA (5 µg) and BLS (60 µg total lipids) were added, and the macrophages were immediately exposed to US. US was generated using a Sonopore-4000 sonicator (NEPA GENE, Chiba, Japan). Then, 1 h later, the incubation medium was replaced with RPMI-1640 and incubated for an additional 23 h. Lipofectamine[®] 2000 (Invitrogen, Carlsbad, CA, USA) was used according to the recommended procedures, and the exposure time of Lipofectamine[®] 2000 was 1 h, which is the same exposure time in other experiments using lipoplexes. Following incubation for 24 h, the cells were scraped from the plates and suspended in lysis buffer (0.05% Triton X-100, 2 mM EDTA, 0.1 M Tris, pH 7.8). Then, the cell suspension was shaken, and centrifuged at 10,000g, 4 °C for 10 min. The supernatant was mixed with luciferase assay buffer (Promega, Tokyo Ink Co., Ltd., Tokyo, Japan) and the luciferase activity was measured in a luminometer (Lumat LB 9507, EG&G Berthold, Bad Wildbad, Germany). The luciferase activity was normalized with respect to the protein content of cells. The protein concentration was determined with a Protein Quantification Kit (Dojindo Molecular Technologies, Inc., Tokyo, Japan). The level of luciferase mRNA expression was determined by RT-PCR.

2.6. Inhibitory experiments of endocytosis in vitro

Endocytosis was inhibited by chlorpromazine (50 µM) as clathrin-mediated endocytosis inhibitor [22], genistein (200 µM) as caveolae-mediated endocytosis inhibitor [23] and 5-(N-ethyl-N-isopropyl)amiloride (EIPA, 50 µM) as macropinosome inhibitor [24]. Each endocytosis inhibitor was added to the macrophages at 30 min before the addition of lipoplexes.

2.7. Fluorescence photographs of pDNA in mouse peritoneal macrophages

To visualize the cellular association of pDNA by fluorescence microscopy (Biozero BZ-8000, KEYENCE, Osaka, Japan), lipoplexes were constructed with Rhodamine-labeled pDNA prepared by a Label IT Nucleic Acid Labeling Kit (Mirus Co., Madison, WI, USA).

2.8. Evaluation of cytotoxic effects by MTT assay

The cytotoxicity was evaluated by MTT assay. Briefly, 3-(4,5-dimethyl-2-thiazol)-2,5-diphenyltetrazolium bromide (MTT, Naacal Tesque, Inc., Kyoto, Japan) solution was added to each well and incubated for 4 h. The resultant formazan crystals were dissolved in 0.04 M HCl-isopropanol and sonicated for 10 min in a bath sonicator. Absorbance values at 550 nm (test wavelength) and 655 nm (reference wavelength) were measured and the results were expressed as viability (%).

2.9. In-vitro gene transfection

Four-week-old ICR female mice were intravenously injected with 400 µl bubble lipoplexes via the tail vein using a 26-gauge syringe needle at a dose of 50 µg pDNA. At 5 min after the injection of bubble lipoplexes, US (frequency, 1.045 MHz; duty, 50%; burst rate, 10 Hz; intensity 1.0 W/cm²; time, 2 min) was exposed transdermally to the abdominal area using a Sonopore-4000 sonicator with a probe of diameter 20 mm. In the transfection using naked pDNA and BLS, at 4 min after intravenous injection of BLS (500 µg total lipid), naked pDNA (50 µg) was intravenously injected and US was exposed at 1 min after naked pDNA injection. At predetermined times after injection, mice were sacrificed and their organs collected for each experiment. The organs were washed twice with cold saline and homogenized with lysis buffer (0.05% Triton X-100, 2 mM EDTA, 0.1 M Tris, pH 7.8). The lysis buffer was added in a weight ratio of 5 mL/g for the liver or 5 mL/g for the other organs. After three cycles of freezing and thawing, the homogenates were centrifuged at 10,000g, 4 °C for

10 min. The luciferase activity of resultant supernatant was determined by luciferase assay and the level of luciferase mRNA expression was determined by RT-PCR.

2.10. In-vivo imaging

At 6 h after transfection, anesthetized mice were administered *o*-luciferin (10 mg/300 µl PBS) (Promega Co., Madison, WI, USA). At 10 min after injection of *o*-luciferin, organs were excised and luminescent images were taken by NightOWL-LB 981 NC instrument (Berthold Technologies, GmbH, Bad Wildbad, Germany). The pseudocolor luminescent images were generated, overlaid with organ images and the luminescence representation was obtained using WinLight software (Berthold Technologies GmbH, Bad Wildbad, Germany).

2.11. Separation of mouse hepatic PCs and NPCs

The separation of mouse hepatic PCs and NPCs was performed according to our previous reports [19]. Briefly, at 6 h after in-vivo transfection using bubble lipoplexes and US exposure, each mouse was anesthetized with pentobarbital sodium (40–60 mg/kg) and the liver was perfused with perfusion buffer (Ca²⁺, Mg²⁺-free HEPES solution, pH 7.2) for 10 min. Then, the liver was perfused with collagenase buffer (HEPES solution, pH 7.5 containing 5 mM CaCl₂ and 0.05% (w/v) collagenase (type I)) for 5 min. Immediately after the start of perfusion, the vena cava and aorta were cut and the perfusion rate was maintained at 5 mL/min. At the end of perfusion, the liver was excised. The cells were dispersed in ice-cold Hank's-HEPES buffer by gentle stirring and then filtered through cotton mesh sieves, followed by centrifugation at 50g for 1 min. The pellets containing the hepatic PCs were washed five times with Hank's-HEPES buffer by centrifuging at 50g for 1 min. The supernatant containing the hepatic NPCs was similarly centrifuged 5 times and the resulting supernatant was centrifuged twice at 300g for 10 min. Then, the PCs and NPCs were resuspended separately in ice-cold Hank's-HEPES buffer.

2.12. Isolation of mouse splenic CD11c⁺ cells

The isolation of mouse splenic CD11c⁺ cells was performed according to our previous reports [25]. Briefly, at 6 h after in-vivo transfection using bubble lipoplexes and US exposure, the splenic cells were suspended in ice-cold RPMI-1640 medium on ice. Red blood cells were removed by incubation with hemolytic reagent (0.15 M NH₄Cl, 10 mM KHCO₃, 0.1 mM EDTA) for 3 min at room temperature. The CD11c⁺ cells were isolated by magnetic cell sorting with anti-mouse CD11c (N418) microbeads and auto MACS (Miltenyi Biotec, Inc., Auburn, CA, USA) following the manufacturer's instructions.

2.13. Quantitative RT-PCR

Total RNA was isolated from separated cells using a GenElute Mammalian Total RNA Miniprep Kit (Sigma-Aldrich, St. Louis, MO, USA). Reverse transcription of mRNA was carried out using a PrimeScript[®] RT reagent kit (Takara Bio Inc., Shiga, Japan). Real-time PCR was performed using SYBR[®] Premix Ex Taq (Takara Bio Inc., Shiga, Japan) and Lightcycler Quick System 350S (Roche Diagnostics, Indianapolis, IN, USA) with primers. The primers for luciferase and gapdh cDNA were constructed as follows: primer for luciferase cDNA, 5'-TTCTTCCGCAAAAGCACTC-3' (forward) and 5'-CCCTCGGTGTAATCAGAAT-3' (reverse); primer for gapdh, 5'-CTCTCCGGCACTT-CAACA-3' (forward) and 5'-GCTGTAGCCGTATTCATTG-3' (reverse) (Sigma-Aldrich, St. Louis, MO, USA). The mRNA copy numbers were calculated for each sample from the standard curve using the instrument software ('Arithmetic Fit Point analysis' for the Lightcycler). The results were expressed as the ratio of luciferase mRNA copy numbers to the housekeeping gene (gapdh) mRNA copy numbers.

2.14. Tissue distribution of radio-labeled pDNA

Lipoplexes constructed with ³²P-labeled pDNA ([³²P]-dCTP, PerkinElmer, Inc., MA, USA) [26] were injected intravenously into mice. At predetermined times after injection, blood was collected from the vena cava under pentobarbital anesthesia. Then, mice were sacrificed and the organs were collected, rinsed with saline and weighed. The tissues were dissolved in Soluene-350 and the resultant lysates were decolorized with isopropanol and 30% H₂O₂, and then neutralized with 5 N HCl. The radioactivity of ³²P-labeled pDNA was measured in scintillation counter (LSA-500, Beckman Coulter, Inc., CA, USA) after addition of Clear-Sol 1 solution.

2.15. Measurement of transaminase activity in the serum

At predetermined times after transfection, the serum was collected from the anesthetized mice. Alanine aminotransferase (ALT) and aspartate aminotransferase (AST) activities in the serum were determined using Transaminase CII-Test Wako kit (Wako Pure, Chemical Industries Ltd., Tokyo, Japan) according to manufacturer's instructions.

2.16. Antigen presenting assay

The evaluation of antigen presentation on MHC class I molecules in the splenic dendritic cells was performed by *in-vitro* antigen presentation assay using CD8-OVA1.3 cells, which are T cell hybridomas with specificity for OVA. The CD11c⁺ cells isolated from immunized mice were plated in a 96-well plate at various cells numbers and co-cultured with CD8-OVA1.3 cells (1×10^5) for 20 h. The antigen presentation on MHC class I molecules was evaluated by IL-2 secreted from activated CD8-OVA1.3 cells measured by a commercial IL-2 ELISA Kit (Bay bioscience Co., Ltd., Hyogo, Japan).

2.17. Evaluation of OVA-specific cytokine secretion from the splenic cells

At 2 weeks after the last immunization, the splenic cells collected from immunized mice were plated in 96-well plates and incubated for predetermined times at 37 °C in the presence or absence of OVA (100 µg). IFN-γ and IL-4 in the culture medium were measured by the commercial ELISA Kit, respectively (Bay bioscience Co., Ltd., Hyogo, Japan).

2.18. OVA-specific CTL assay

At 2 weeks after the last immunization, the splenic cells harvested from immunized mice were plated in 6-well plates and co-cultured with mitomycin C-treated E.G7-OVA cells or EL4 cells for 4 days. After co-incubation, non-adherent cells were collected, washed and plated in 96-well plates with target cells (E.G7-OVA cells or EL4 cells) at various effector/target (E/T) ratios. The target cells were labeled with ⁵¹Cr by incubating with Na²⁵¹CrO₄ (PerkinElmer, Inc., MA, USA) in culture medium for 1 h at 37 °C. At 4 h after incubation, the plates were centrifuged and the resultant supernatant of each well was collected and the radioactivity of released

⁵¹Cr was measured in a gamma counter. The percentage of ⁵¹Cr release was calculated as follows: specific (lysis (%)) = [(experimental ⁵¹Cr release – spontaneous ⁵¹Cr release)/(maximum ⁵¹Cr release – spontaneous ⁵¹Cr release)] × 100. The percentage of OVA-specific ⁵¹Cr release was calculated as (% of ⁵¹Cr release from E.G7-OVA cells) – (% of ⁵¹Cr release from EL4 cells).

2.19. Therapeutic effects

C57BL/6 mice were immunized three times biweekly. At 2 weeks after last immunization, E.G7-OVA cells and EL4 cells were transplanted subcutaneously into the back of mice. The tumor growth and survival of mice were monitored up to 80 days after transplantation of E.G7-OVA cells and EL4 cells.

2.20. Statistics

Results were presented as the mean ± SD of more than three experiments. Analysis of variance (ANOVA) was used to test the statistical significance of differences among groups. Two-group comparisons were performed by the Student's *t*-test. Multiple comparisons between control groups and other groups were performed by the Dunnett's test and multiple comparisons between all groups were performed by the Tukey-Kramer test.

3. Results

3.1. *In-vitro* gene transfection properties by Man-PEG₂₀₀₀ lipoplexes

Polyethylene-glycol (PEG) modification of particles is necessary to enclose US imaging gas stably and to prepare the

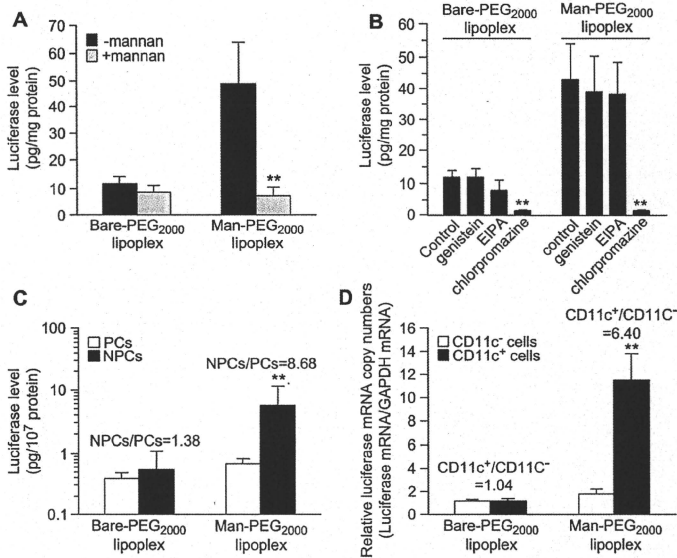


Fig. 2. The mannose receptor-expressing cell-selective gene expression by Man-PEG₂₀₀₀ lipoplexes containing Man-PEG₂₀₀₀ lipids *in vitro* and *in vivo*. (A) The level of luciferase expression obtained by Bare-PEG₂₀₀₀ lipoplexes and Man-PEG₂₀₀₀ lipoplexes (5 µg pDNA) in the absence or presence of 1 mg/ml mannans in mouse cultured macrophages at 24 h after transfection. ***p* < 0.01, compared with the corresponding group of mannans. (B) Inhibition of luciferase expression obtained by Bare-PEG₂₀₀₀ lipoplexes and Man-PEG₂₀₀₀ lipoplexes (5 µg pDNA) in addition of various endocytosis inhibitors in mouse cultured macrophages at 24 h after transfection. ***p* < 0.01, compared with the corresponding group of control. (C) The level of luciferase expression in mouse hepatic PCs and NPCs after intravenous administration of Bare-PEG₂₀₀₀ lipoplexes and Man-PEG₂₀₀₀ lipoplexes (50 µg pDNA) in mice at 6 h after transfection. ***p* < 0.01, compared with the corresponding group of PCs. (D) The level of luciferase mRNA expression in mouse splenic CD11c⁺ cells and CD11c⁻ cells after intravenous administration of Bare-PEG₂₀₀₀ lipoplexes and Man-PEG₂₀₀₀ lipoplexes (50 µg pDNA) in mice at 6 h after transfection. ***p* < 0.01, compared with the corresponding group of CD11c⁻ cells. Each value represents the mean ± SD (*n* = 3–4).

small-sized microbubbles for in-vivo administration [12]. Firstly, we developed mannose-conjugated PEG₂₀₀₀-modified lipids (Man-PEG₂₀₀₀-DSPE (Fig. 1)) to prepare the APC-targeted small-sized microbubbles and determined the in-vitro and in-vivo transfection characteristics of mannose-conjugated PEG₂₀₀₀-modified lipoplexes (Man-PEG₂₀₀₀ lipoplexes) containing Man-PEG₂₀₀₀ lipids. The particle sizes and zeta potentials of Man-PEG₂₀₀₀ lipoplexes and non-modified PEG₂₀₀₀-lipoplexes (Bare-PEG₂₀₀₀ lipoplexes) were approximately 150 nm and +40 mV, respectively (Supplementary Table 1). In mouse cultured macrophages expressing mannose receptors abundantly, the level of gene expression obtained by Man-PEG₂₀₀₀ lipoplexes were significantly higher than those by Bare-PEG₂₀₀₀ lipoplexes (Fig. 2A and B). Then, the level of gene expression obtained by Man-PEG₂₀₀₀ lipoplexes was suppressed to same extent as that by Bare-PEG₂₀₀₀ lipoplexes in the presence of an excess of mannan (Fig. 2A). Moreover, this level of gene expression obtained by Man-PEG₂₀₀₀ lipoplexes was also suppressed to same extent as that by Bare-PEG₂₀₀₀ lipoplexes in the presence of chlorpromazine (Fig. 2B), which is the inhibitor of clathrin-mediated endocytosis [22]. These results agreed with the results of cellular association of pDNA (Supplementary Fig. 1), and suggest that Man-PEG₂₀₀₀ lipoplexes are taken up into the cells via clathrin-mediated endocytosis following the interaction with mannose receptors.

3.2. In-vivo gene transfection properties by Man-PEG₂₀₀₀ lipoplexes

Since the degradation of pDNA by nuclease in the blood is one of the critical factors in the in-vivo gene transfection by intravenously administration of lipoplexes, we investigated the stability of Bare-PEG₂₀₀₀ lipoplexes and Man-PEG₂₀₀₀ lipoplexes against nucleases. Following electrophoresis of naked pDNA and lipoplexes after incubation with DNase I, although naked pDNA underwent the degradation by DNase I, lipoplexes did not undergo the degradation and retained the complex forms (Supplementary Fig. 2). Then, we investigated the gene expression characteristics of Man-PEG₂₀₀₀ lipoplexes in the liver and spleen, which are the targeted organs of mannose-modified carriers [27]. In this study, liver was separated in the parenchymal cells (PCs) and non-parenchymal cells (NPCs), and spleen was separated in the dendritic cells (CD11c⁺ cells) and other cells (CD11c⁻ cells). As shown in Fig. 2C and D, following intravenous administration of Man-PEG₂₀₀₀ lipoplexes, selective gene expression was observed in the hepatic NPCs and the splenic CD11c⁺ cells, which are the APCs expressing mannose receptors abundantly [28–30].

3.3. In-vitro gene transfection efficiency by Man-PEG₂₀₀₀ bubble lipoplexes and US exposure

Although Man-lipoplexes showed the APC-selective gene transfection properties in vivo, this level of gene expression was

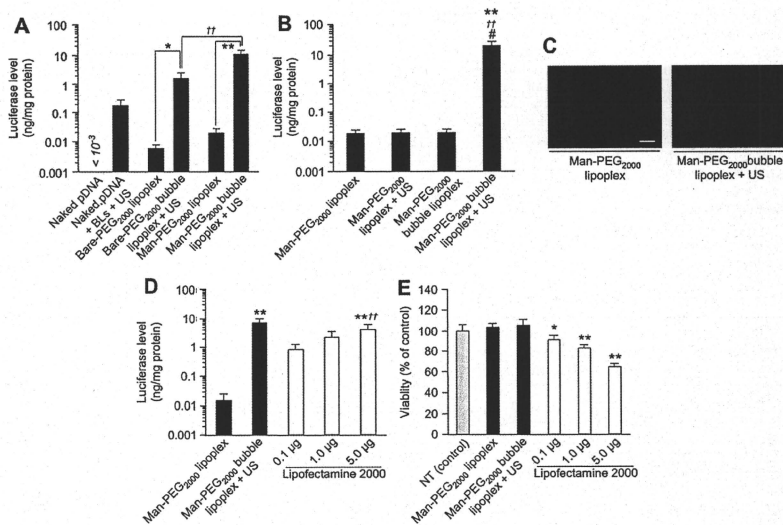


Fig. 3. Enhancement of gene expression by Man-PEG₂₀₀₀ bubble lipoplexes and US exposure in vitro. (A) The level of luciferase expression obtained by naked pDNA, naked pDNA + BLs with US exposure, Bare-PEG₂₀₀₀ lipoplexes, Bare-PEG₂₀₀₀ bubble lipoplexes with US exposure, Man-PEG₂₀₀₀ lipoplexes and Man-PEG₂₀₀₀ bubble lipoplexes with US exposure (5 μg pDNA) at 24 h after transfection. Significant difference; **p* < 0.05; ***p* < 0.01. (B) The level of luciferase expression obtained by Man-PEG₂₀₀₀ lipoplexes and Man-PEG₂₀₀₀ bubble lipoplexes with or without US exposure (5 μg pDNA) at 24 h after transfection. ***p* < 0.01, compared with Man-PEG₂₀₀₀ lipoplex. †*p* < 0.01, compared with Man-PEG₂₀₀₀ bubble lipoplex. ††*p* < 0.01, compared with Man-PEG₂₀₀₀ bubble lipoplex + US. †††*p* < 0.01, compared with Man-PEG₂₀₀₀ lipoplex + US. (C) Representative fluorescent images of cellular association of pDNA obtained by Man-PEG₂₀₀₀ lipoplexes and Man-PEG₂₀₀₀ bubble lipoplexes with US exposure (5 μg pDNA) at 2 h after treatment. Lipoplexes were constructed with TM-rhodamine-labeled pDNA. TM-rhodamine-labeled pDNA (red), nuclei counterstained by DAPI (blue). Scale bars, 100 μm. (D) Comparison of the level of luciferase expression obtained by Man-PEG₂₀₀₀ bubble lipoplexes (5 μg pDNA) and US exposure with that by Lipofectamine 2000. ***p* < 0.01, compared with Man-PEG₂₀₀₀ lipoplexes. †*p* < 0.01, compared with Lipofectamine 2000 (0.1 μg). (E) Comparison of cell viability by transfection using Man-PEG₂₀₀₀ bubble lipoplexes (5 μg pDNA) and US exposure with that by Lipofectamine 2000. N.T., non-treatment. **p* < 0.05; ***p* < 0.01, compared with N.T. Each value represents the mean ± SD (*n* = 4).

low compared with our previous reports [1,19,25]. To enhance the level of gene expression by sonoporation method, we developed Man-PEG₂₀₀₀ bubble lipoplexes (Fig. 1) by enclosing US imaging gas (perfluoropropane gas) into Man-PEG₂₀₀₀ lipoplexes. The lipid composition of lipoplexes is important for the stable enclosure of US imaging gas. Following optimization of lipid composition, lipoplexes constructed with the saturated lipids only, which have a high melting temperature (T_m), were enclosed US imaging gas stably (Supplementary Table 2). Following enclosure of US imaging gas in lipoplexes, lipoplexes became cloudy and their particle sizes were increased (from 150 nm to 550 nm, approximately) (Supplementary Fig. 3A and Table 3). Then, since the zeta potentials of bubble lipoplexes were lower than that of bubble liposomes and same as that of lipoplexes (Supplementary Tables 1 and 3), it is considered that pDNA is attached on the surface of bubble liposomes. Moreover, the stability against nucleases observed in Man-PEG₂₀₀₀ lipoplexes (Supplementary Fig. 2) was maintained after enclosure of US imaging gas into lipoplexes (Supplementary Fig. 3B).

The level of gene expression obtained by Man-PEG₂₀₀₀ bubble lipoplexes and US exposure was 500-fold higher than that by Man-PEG₂₀₀₀ lipoplexes in mouse cultured macrophages expressing mannose receptors abundantly, and also higher than that by non-modified bubble lipoplexes (Bare-PEG₂₀₀₀ bubble lipoplexes, Fig. 1) and US exposure or conventional sonoporation method using naked pDNA and BLs (Fig. 3A). This enhanced gene expression was observed when bubble lipoplexes and US exposure were used for in-vitro gene transfer (Fig. 3B). The cellular association of pDNA obtained by transfection using Man-PEG₂₀₀₀ bubble lipoplexes and US exposure was also 10-fold higher than that by Man-PEG₂₀₀₀ lipoplexes, and also higher than that by Bare-PEG₂₀₀₀ bubble lipoplexes and US exposure or conventional sonoporation method using naked pDNA and BLs (Fig. 3C and Supplementary Fig. 4A). Moreover, this level of gene expression obtained by Man-PEG₂₀₀₀ bubble lipoplexes and US exposure was comparable to that by Lipofectamine® 2000, which is widely used as a gene transfection reagent (Fig. 3D). On the other hand, the cytotoxicity by Man-PEG₂₀₀₀ bubble lipoplexes and US exposure was lower than that by Lipofectamine® 2000 (Fig. 3E).

3.4. Intracellular uptake properties of pDNA by Man-PEG₂₀₀₀ bubble lipoplexes and US exposure

The gene expression obtained by Man-PEG₂₀₀₀ bubble lipoplexes and US exposure was significantly suppressed in the presence of an excess of mannose (Fig. 4A). Therefore, the interaction with mannose receptors on the cell membrane is involved in the gene transfection by Man-PEG₂₀₀₀ bubble lipoplexes and US exposure, similar to the gene transfection by Man-PEG₂₀₀₀ lipoplexes. On the other hand, unlike Man-PEG₂₀₀₀ lipoplexes (Fig. 2B), the gene expression obtained by Man-PEG₂₀₀₀ bubble lipoplexes and US exposure was not suppressed in the presence of chlorpromazine (Fig. 4B), which is a clathrin-mediated endocytosis inhibitor [22]. These results agreed with the results of cellular association of pDNA (Supplementary Fig. 4B), and indicated that pDNA delivered by Man-PEG₂₀₀₀ bubble lipoplexes was directly introduced into the cytoplasm without mediating endocytosis by the gene transfection using Man-PEG₂₀₀₀ bubble lipoplexes and US exposure.

3.5. In-vivo gene transfection efficiency by Man-PEG₂₀₀₀ bubble lipoplexes and US exposure

As shown in Fig. 5A and B, the level of gene expression obtained by Man-PEG₂₀₀₀ bubble lipoplexes and US exposure was

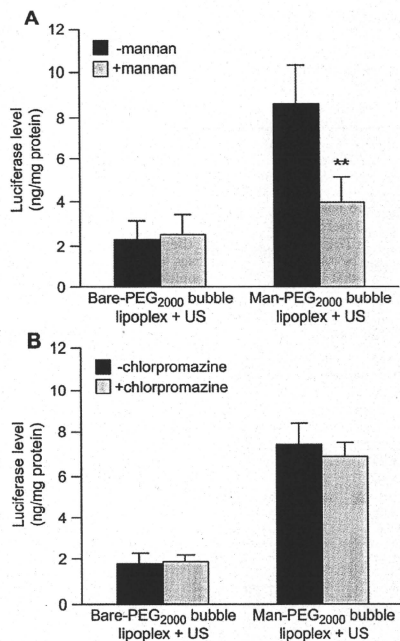


Fig. 4. Effects of mannose and chlorpromazine on gene expression by Man-PEG₂₀₀₀ bubble lipoplexes and US exposure in vitro. (A) The level of luciferase expression obtained by Bare-PEG₂₀₀₀ bubble lipoplexes with US exposure and Man-PEG₂₀₀₀ bubble lipoplexes with US exposure (5 μ g pDNA) in the absence or presence of 1 mg/mL mannose at 24 h after transfection. ** $p < 0.01$, compared with the corresponding group of mannose. (B) The level of luciferase expression by Bare-PEG₂₀₀₀ bubble lipoplexes with US exposure and Man-PEG₂₀₀₀ bubble lipoplexes with US exposure (5 μ g pDNA) in the absence or presence of 50 μ M chlorpromazine at 24 h after transfection. Each value represents the mean \pm SD ($n = 4$).

500–800-fold higher than that by Man-PEG₂₀₀₀ lipoplexes, and also higher than that by Bare-PEG₂₀₀₀ bubble lipoplexes and US exposure or the conventional sonoporation method using naked pDNA and BLs in the liver and spleen, which are the targeted organs of mannose-modified carriers [27]. This enhanced gene expression in the liver and spleen was observed when bubble lipoplexes and US exposure were used for in-vivo gene transfer (Fig. 5C and D). Moreover, this gene expression obtained by Bare-PEG₂₀₀₀ bubble lipoplexes with US exposure or Man-PEG₂₀₀₀ bubble lipoplexes with US exposure in the liver and spleen remained higher than that by Bare-PEG₂₀₀₀ lipoplexes or Man-PEG₂₀₀₀ lipoplexes for at least 48 h, respectively (Fig. 5E and F). In addition, the gene expression was also enhanced in the US-exposed organ specifically following gene transfection by direct US exposure to the targeted organ after intravenous administration of Man-PEG₂₀₀₀ bubble lipoplexes (Supplementary Fig. 5). On the other hand, the increase of gene expression by bubble lipoplexes and US exposure was not observed in other organ such as lung, kidney and heart (Fig. 5G and H).

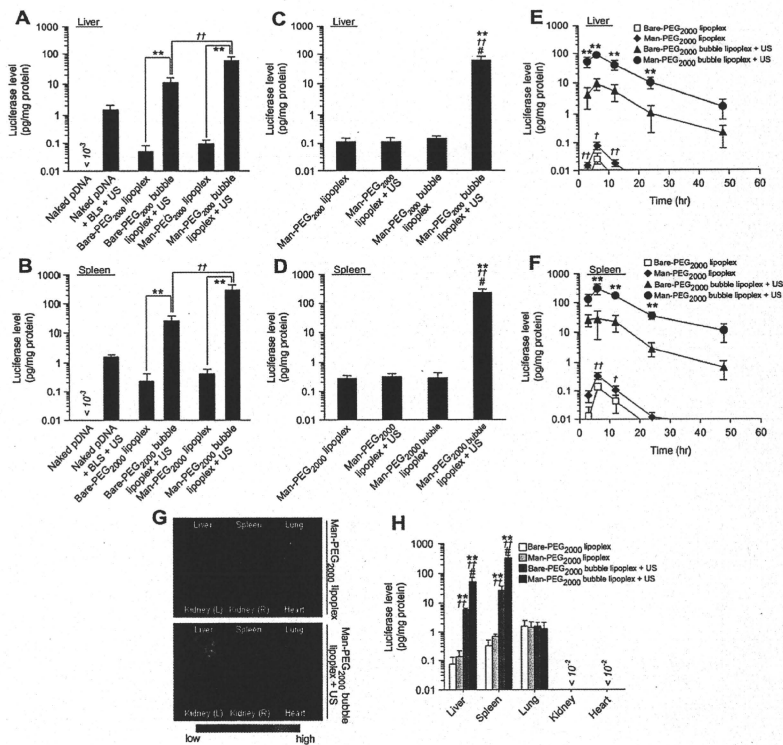


Fig. 5. Enhancement of mannose receptor-expressing cells-selective gene expression by Man-PEG₂₀₀₀ bubble lipoplexes and US exposure in vivo. (A, B) The level of luciferase expression obtained by naked pDNA, naked pDNA + BLs with US exposure, Bare-PEG₂₀₀₀ lipoplexes, Bare-PEG₂₀₀₀ bubble lipoplexes with US exposure, Man-PEG₂₀₀₀ lipoplexes and Man-PEG₂₀₀₀ bubble lipoplexes with US exposure (50 μ g pDNA) in the liver (A) and spleen (B) at 6 h after transfection. Significant difference: ** $p < 0.01$, compared with the corresponding group of Man-PEG₂₀₀₀ lipoplex + US. (C, D) The level of luciferase expression obtained by Man-PEG₂₀₀₀ lipoplexes and Man-PEG₂₀₀₀ bubble lipoplexes with or without US exposure (50 μ g pDNA) in the liver (C) and spleen (D) at 6 h after transfection. ** $p < 0.01$, compared with Man-PEG₂₀₀₀ lipoplex; # $p < 0.01$, compared with Man-PEG₂₀₀₀ lipoplex + US; $\eta p < 0.01$, compared with Man-PEG₂₀₀₀ bubble lipoplex. (E, F) Time-course of luciferase expression in the liver (E) and spleen (F) after transfection by Bare-PEG₂₀₀₀ lipoplexes, Man-PEG₂₀₀₀ lipoplexes, Bare-PEG₂₀₀₀ bubble lipoplexes with US exposure and Man-PEG₂₀₀₀ bubble lipoplexes with US exposure (50 μ g pDNA). Each value represents the mean \pm SD ($n = 4$). ** $p < 0.01$, compared with Bare-PEG₂₀₀₀ bubble lipoplex + US; # $p < 0.05$; $\eta p < 0.01$, compared with Bare-PEG₂₀₀₀ lipoplex. (G) In-vivo imaging photographs of luciferase expression in the isolated organs at 6 h after transfection by Man-PEG₂₀₀₀ lipoplexes and Man-PEG₂₀₀₀ bubble lipoplexes with US exposure (50 μ g pDNA). (H) The level of luciferase expression in each organ at 6 h after transfection by Bare-PEG₂₀₀₀ lipoplexes, Man-PEG₂₀₀₀ lipoplexes, Bare-PEG₂₀₀₀ bubble lipoplexes with US exposure and Man-PEG₂₀₀₀ bubble lipoplexes with US exposure (50 μ g pDNA). ** $p < 0.01$, compared with the corresponding group of Bare-PEG₂₀₀₀ lipoplex; # $p < 0.01$, compared with the corresponding group of Man-PEG₂₀₀₀ lipoplex; $\eta p < 0.01$, compared with the corresponding group of Bare-PEG₂₀₀₀ bubble lipoplex + US. Each value represents the mean \pm SD ($n = 4$).

3.6. Targeted cell-selective gene transfection properties by Man-PEG₂₀₀₀ bubble lipoplexes and US exposure in vivo

We investigated the mannose receptor-expressing cell selectivity of gene expression by transfection using Man-PEG₂₀₀₀ bubble lipoplexes and US exposure. In the liver, the level of gene expression in the hepatic NPCs expressing mannose receptors was significantly higher than that in the hepatic PCs following gene transfection by Man-PEG₂₀₀₀ bubble lipoplexes and US exposure (Fig. 6A). This difference in gene expression between the NPCs and PCs obtained by Man-PEG₂₀₀₀ bubble lipoplexes and US exposure

was similar to that by Man-PEG₂₀₀₀ lipoplexes, although the level of gene expression in the NPCs and PCs was markedly higher. On the other hand, selective gene expression in the NPCs was not observed by Bare-PEG₂₀₀₀ bubble lipoplexes and US exposure.

In the spleen, the level of mRNA expression in the CD11c⁺ cells, which are the splenic dendritic cells expressing mannose receptors, was significantly higher than that in the CD11c⁻ cells following transfection by Man-PEG₂₀₀₀ bubble lipoplexes and US exposure (Fig. 6B). On the other hand, selective gene expression in the CD11c⁺ cells was not observed by Bare-PEG₂₀₀₀ bubble lipoplexes and US exposure.

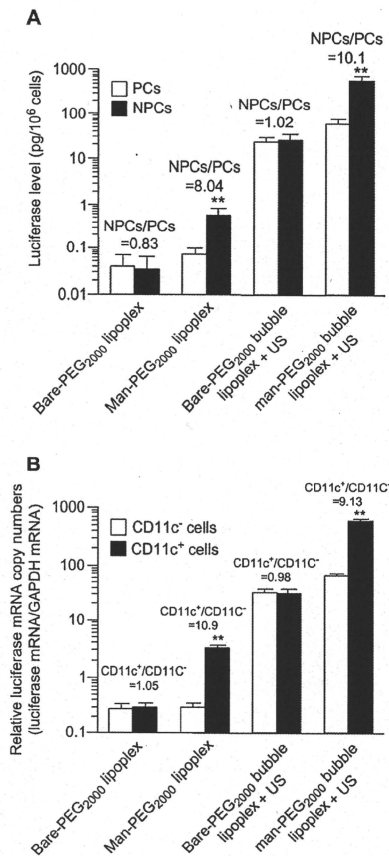


Fig. 6. Hepatic and splenic cellular localization of luciferase expression by Man-PEG₂₀₀₀ bubble lipoplexes and US exposure. (A) Hepatic cellular localization of luciferase expression at 6 h after transfection by Bare-PEG₂₀₀₀ lipoplexes, Man-PEG₂₀₀₀ lipoplexes, Bare-PEG₂₀₀₀ bubble lipoplexes with US exposure and Man-PEG₂₀₀₀ bubble lipoplexes with US exposure (50 μ g pDNA). ** $p < 0.01$, compared with the corresponding group of PCs. (B) Splenic cellular localization of luciferase mRNA expression at 6 h after transfection by Bare-PEG₂₀₀₀ lipoplexes, Man-PEG₂₀₀₀ lipoplexes, Bare-PEG₂₀₀₀ bubble lipoplexes with US exposure and Man-PEG₂₀₀₀ bubble lipoplexes with US exposure (50 μ g pDNA). ** $p < 0.01$, compared with the corresponding group of CD11c⁺ cells. Each value represents the mean \pm SD ($n = 4$).

3.7. In-vivo distribution properties of pDNA by Man-PEG₂₀₀₀ bubble lipoplexes and US exposure

Next, to elucidate the mechanism of enhanced in-vivo gene expression using Man-PEG₂₀₀₀ bubble lipoplexes and US exposure, we investigated the effect on the tissue distribution of pDNA followed by gene transfection. In this study, Bare-PEG₂₀₀₀ bubble lipoplexes

and Man-PEG₂₀₀₀ bubble lipoplexes constructed with radio-labeled pDNA were intravenously administered, and then mice were subjected to external US exposure. As shown in Fig. 7, in the case of both bubble lipoplexes, the retention time of pDNA in the blood was slightly reduced and the distribution of pDNA delivered by bubble lipoplexes was significantly increased by US exposure in the liver and spleen (Fig. 7). Moreover, the amount of pDNA distributed in the liver and spleen by Man-PEG₂₀₀₀ bubble lipoplexes and US exposure (Fig. 7A) was higher than that by Bare-PEG₂₀₀₀ bubble lipoplexes and US exposure (Fig. 7B). On the other hand, no increase of pDNA distribution followed by US exposure was observed in the lung.

3.8. The liver toxicity by Man-PEG₂₀₀₀ bubble lipoplexes and US exposure

We examined ALT and AST activities in the serum to investigate the liver toxicity by gene transfection using Man-PEG₂₀₀₀ bubble lipoplexes and US exposure. ALT and AST activities in the serum were increased by gene transfection using Bare-PEG₂₀₀₀ lipoplexes and Man-PEG₂₀₀₀ lipoplexes. On the other hands, the increase of ALT and AST activities was not observed by gene transfection using Bare-PEG₂₀₀₀ bubble lipoplexes and Man-PEG₂₀₀₀ bubble lipoplexes with US exposure (Fig. 8).

3.9. Antigen presentation on MHC class I molecules in immunized splenic dendritic cells

To investigate the DNA vaccine effects by Man-PEG₂₀₀₀ bubble lipoplexes and US exposure, we prepared Man-PEG₂₀₀₀ bubble lipoplexes constructed with pDNA expressing OVA as a model antigen. Firstly, to investigate the antigen (OVA) presentation on MHC class I molecules in the splenic dendritic cells (CD11c⁺ cells) by Man-PEG₂₀₀₀ bubble lipoplexes constructed with pCMV-OVA and US exposure, the splenic CD11c⁺ cells isolated from once-immunized mice were co-incubated with CD8-OVA13 cells, which are T cell hybridomas with specificity for OVA. Following measurement of IL-2 to evaluate the activation of T cells, the IL-2 secretion from activated CD8-OVA13 cells co-incubated with the CD11c⁺ cells isolated from mice immunized by Man-PEG₂₀₀₀ bubble lipoplexes and US exposure was the highest of all (Fig. 9A). This result indicates that DNA vaccination by Man-PEG₂₀₀₀ bubble lipoplexes constructed with pCMV-OVA and US exposure can induce significantly high CD8⁺-T lymphocyte activation.

3.10. Antigen-specific cytokine secretion from immunized splenic cells

We evaluated the OVA-specific cytokine secretion from the splenic cells immunized by Man-PEG₂₀₀₀ bubble lipoplexes constructed with pCMV-OVA and US exposure. Following optimization of immunization schedule, it was shown that a 2 week interval was necessary to achieve the same level of gene expression as former transfection in the spleen (Supplementary Fig. 6) and at least three times immunization was necessary to effective anti-tumor effects by DNA vaccination using this method (Supplementary Fig. 7). Therefore, the immunization to mice was performed according to the protocol shown in Fig. 9B. As shown in Fig. 9C, in the presence of OVA, the highest amount of IFN- γ (Th1 cytokine) was secreted from splenic cells harvested from mice immunized with Man-PEG₂₀₀₀ bubble lipoplexes and US exposure. On the other hand, no secretion of IFN- γ was observed in any of the groups in the absence of OVA. Moreover, the secretion of IL-4 (Th2 cytokine) was not increased in any of the groups both in the presence or absence of OVA (Fig. 9C). These results suggest that immunization by Man-PEG₂₀₀₀ bubble lipoplexes constructed with

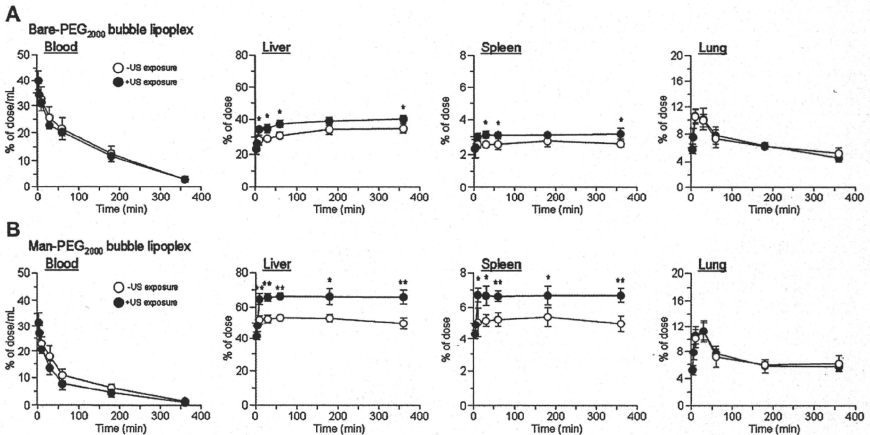


Fig. 7. Tissue distribution of pDNA by Man-PEG₂₀₀₀ bubble lipoplexes and US exposure. Tissue distribution after intravenous administration of (A) Bare-PEG₂₀₀₀ bubble lipoplexes and (B) Man-PEG₂₀₀₀ bubble lipoplexes (50 μ g pDNA) with or without US exposure in mice. US was exposed at 5 min after intravenous administration of bubble lipoplexes. Each value represents the mean \pm SD ($n = 3$). * $p < 0.05$; ** $p < 0.01$, compared with the corresponding group of US exposure.

pCMV-OVA and US exposure significantly enhances the differentiation of helper T cells to Th1 cells, which are pivotal cells for the activation of cytotoxic T lymphocytes (CTL) with high anti-tumor activity, by OVA stimulation.

3.11. Antigen-expressing cell-specific CTL activity in immunized splenic cells

Next, we assessed the CTL activity in the splenic cells harvested from mice immunized by Man-PEG₂₀₀₀ bubble lipoplexes and US exposure. Following experiments according to the protocol shown in Fig. 9B, the splenic cells immunized by Man-PEG₂₀₀₀ bubble lipoplexes constructed with pCMV-OVA and US exposure showed the highest CTL activity in all groups against E.G7-OVA cells which are the lymphoma cells expressing OVA (Fig. 9D). In contrast, the CTL activity was not observed in EL4 cells which are the lymphoma cells not expressing OVA in all groups (Fig. 9D). These results indicate that the splenic cells immunized by Man-PEG₂₀₀₀ bubble lipoplexes constructed with pCMV-OVA and US exposure induce the OVA-expressing cell-specific CTL activity.

3.12. Therapeutic effects against antigen-expressing tumor by DNA vaccination

Finally, we investigated the anti-tumor effects by DNA vaccination using Man-PEG₂₀₀₀ bubble lipoplexes and US exposure. Following experiments according to the protocol shown in Fig. 10A, significantly high anti-tumor effects against E.G7-OVA cells were observed in mice immunized by Man-PEG₂₀₀₀ bubble lipoplexes constructed with pCMV-OVA and US exposure (Fig. 10B). However, in mice transplanted EL4 cells, no anti-tumor effects were observed in any of the groups (Fig. 10C). Moreover, we investigated the maintenance of DNA vaccine effects following administration of Man-PEG₂₀₀₀ bubble lipoplexes and US exposure. According to the protocol shown in Fig. 11A, E.G7-OVA cells were re-transplanted

into mice which first-transplanted tumors were completely rejected by DNA vaccination using Man-PEG₂₀₀₀ bubble lipoplexes and US exposure. As results, high anti-tumor effects were observed in mice following re-transplantation of E.G7-OVA cells (Fig. 11B); therefore it was demonstrated that DNA vaccine effects obtained by Man-PEG₂₀₀₀ bubble lipoplexes constructed with pCMV-OVA and US exposure were maintained for at least 80 days.

4. Discussion

To obtain high therapeutic effects by DNA vaccination using tumor-specific antigen-coding gene, it is essential to transfer the gene selectively and efficiently into the APCs, such as macrophages and dendritic cells [31,32]. However, it is difficult to transfer the gene into the APCs selectively because of the number of APCs is limited in the organ [33]. Since the APCs are expressed a large number of mannose receptors [28,29], we and other groups have developed mannose-modified non-viral carriers for gene delivery to the APCs [7,25,34]. On the other hand, our group also reported that the gene transfection efficiency in the APCs was lower than that in other cells [35]; therefore it is difficult to achieve high gene transfection efficiency to induce high therapeutic effects by DNA vaccination *in vivo*. In the present study, to establish an APC-selective and efficient gene delivery system, we developed US-responsive and mannose-modified carriers, named Man-PEG₂₀₀₀ bubble lipoplexes, which had selectivity to the APCs and responded to US exposure. The gene delivery system using Man-PEG₂₀₀₀ bubble lipoplexes and US exposure enabled to achieve markedly high gene expression in macrophages and dendritic cells selectively *in vivo*, in spite of the handy system used intravenous administration and external US exposure. Moreover, we succeeded in obtaining high anti-tumor effects by applying this method to DNA vaccine therapy using OVA-expressing pDNA.

Firstly, since PEG₂₀₀₀-modification is necessary to enclose US imaging gas stably [12], we prepared Man-PEG₂₀₀₀ lipoplexes

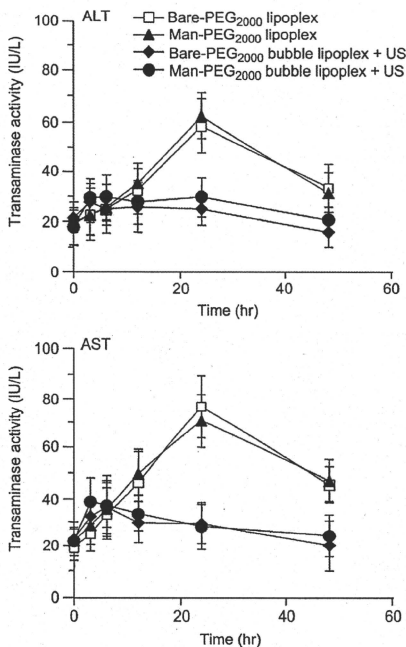


Fig. 8. Liver toxicity by gene transfection using Man-PEG₂₀₀₀ bubble lipoplexes and US exposure. Time-course of serum transaminase activities after transfection by Bare-PEG₂₀₀₀ lipoplexes, Man-PEG₂₀₀₀ lipoplexes, Bare-PEG₂₀₀₀ bubble lipoplexes with US exposure and Man-PEG₂₀₀₀ bubble lipoplexes with US exposure (50 μ g pDNA). Alanine aminotransferase (ALT) and aspartate aminotransferase (AST) in the serum were measured at predetermined times after transfection. Each value represents the mean \pm SD ($n = 4$).

containing Man-PEG₂₀₀₀ lipids. This Man-PEG₂₀₀₀ lipoplexes exhibited mannose receptor-expressing cell-selective gene expression both *in vitro* and *in vivo* (Fig. 2). On the other hand, the level of gene expression by Man-PEG₂₀₀₀ lipoplexes was lower than that by mannose lipoplexes without PEG-modification, as reported previously by our group [1,25]. However, this result was considered to be contributed by the reduced interaction with the cell membrane and the reduction of endosomal escape efficiency by PEG₂₀₀₀-modification [36,37]. In the sonoporation method, Tachibana et al. demonstrated that a transient pore is created on the cell membrane followed by the degradation of microbubbles [38]. Then, nucleic acids, such as pDNA, siRNA and oligonucleotides, are introduced into the cell through the generated pore [13,15,16]. Consequently, since the nucleic acids are directly introduced into cytoplasm in the sonoporation method [13,14], it is considered that the low level of transfection efficiency obtained by Man-PEG₂₀₀₀ lipoplexes can be overcome by applying sonoporation method. As shown in Figs. 3 and 4, a large amount of pDNA is directly introduced into the cytoplasm and high level of gene expression is observed by gene transfection using Man-PEG₂₀₀₀ bubble

lipoplexes and US exposure. Therefore, by delivering pDNA to the APCs using Man-PEG₂₀₀₀ bubble lipoplexes, it is suggested that high level of gene expression in the APCs can easily achieve by following US exposure in this gene transfection method.

In this study, the level of gene expression obtained by transfection using Man-PEG₂₀₀₀ bubble lipoplexes and US exposure was higher than that obtained by Man-PEG₂₀₀₀ lipoplexes or Bare-PEG₂₀₀₀ bubble lipoplexes with US exposure in the liver and spleen (Fig. 5). Moreover, gene expression by Man-PEG₂₀₀₀ bubble lipoplexes and US exposure was observed selectively in the hepatic NPCs and the splenic dendritic cells (Fig. 6), known as mannose receptor-expressing cells [28–30]. Although this selectivity of gene expression was the same as that obtained by mannose lipoplexes reported previously by our group [1,25], this level of gene expression was markedly higher. It is considered that this enhanced and cell-selective gene expression is contributed by the increase of interaction with mannose receptor-expressing cells by mannose modification (Supplementary Fig. 1), by the improvement of delivering efficiency of nucleic acids to the targeted organs (Fig. 7) and by the direct introduction of nucleic acids into the cytoplasm of targeted cells followed by US exposure to Man-PEG₂₀₀₀ bubble lipoplexes (Figs. 3C and 4B and Supplementary Fig. 4). Moreover, the enhanced gene expression was not observed in the lung, kidney and spleen (Fig. 5G and H). It is guessed that the reason why the enhanced gene expression was not observed in the lung is because US is not spread to the thoracic cavity by the diaphragm, and the reason why the enhanced gene expression was not observed in the kidney and heart was because the distributed amounts of bubble lipoplexes were markedly small. In addition, since the particle size of bubble lipoplexes (approximately 500 nm) is suitable for delivery to the liver and spleen, compared with stabilized liposomes (approximately 100 nm) [39], the gene transfection system using Man-PEG₂₀₀₀ bubble lipoplexes and US exposure is a suitable method for the selective delivery of nucleic acids into the mannose receptor-expressing cells in the liver and spleen.

On the other hand, the liver toxicity followed by gene transfection using Man-PEG₂₀₀₀ bubble lipoplexes and US exposure was lower than that by Man-PEG₂₀₀₀ lipoplexes (Fig. 8). It was reported that the CpG motifs in the pDNA sequence are recognized to Toll-like receptor 9 (TLR9) in the endosomes [40,41]; therefore it has been considered that the production of proinflammatory cytokines, such as TNF- α , IFN- γ and IL-12, could be induced in the lipofection method using liposomes and emulsions, and these cytokines cause liver injury [42]. However, in the gene transfection using Man-PEG₂₀₀₀ bubble lipoplexes and US exposure, a large amount of pDNA was directly introduced into the cytoplasm not-mediated endocytosis (Figs. 3C and 4B and Supplementary Fig. 4). Therefore, it is considered that pDNA is not recognized to TLR9 in the endosomes, and consequently liver toxicity followed by transfection using Man-PEG₂₀₀₀ bubble lipoplexes and US exposure is low.

In the previous study [16], we developed combination-use method using mannose lipoplexes [1] and BLS [12] with US exposure to achieve targeted cell-selective gene transfer. However, this combination-use method is complicated because of the necessity of twice injection of mannose lipoplexes and BLS, therefore it is difficult to apply for medical treatments using multiple injection. Moreover, it is considered that the difference of *in-vivo* distribution characteristics between mannose lipoplexes and BLS might be decreased its transfection efficiency. On the other hand, this transfection method using Man-PEG₂₀₀₀ bubble lipoplexes and US exposure is handy because of using only once injection of Man-PEG₂₀₀₀ bubble lipoplexes and external US exposure. In addition, this method using Man-PEG₂₀₀₀ bubble lipoplexes and US exposure overcame the difference of *in-vivo* distribution of formulations, which might lead to the decrease of

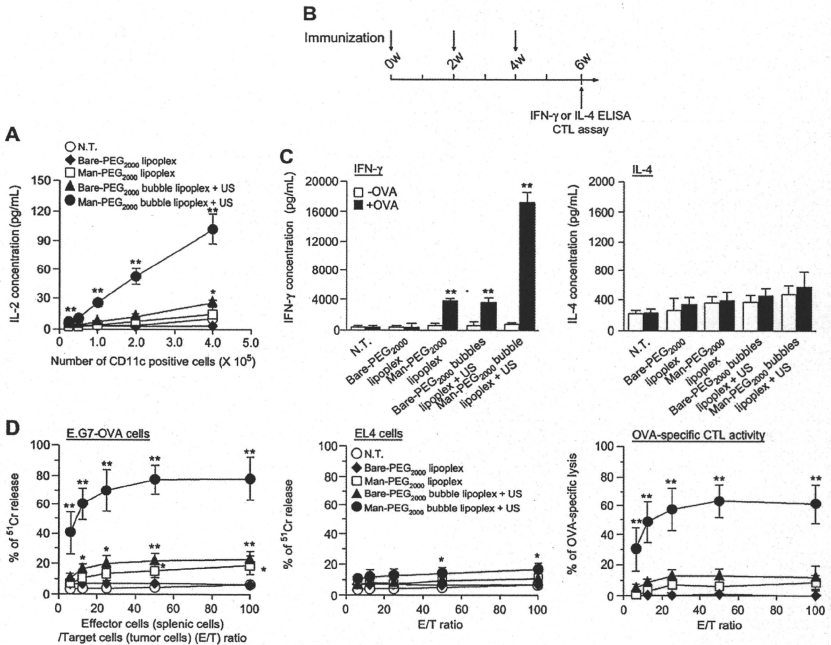


Fig. 9. Cytokine secretion characteristics and CTL activities by DNA vaccination using Man-PEG₂₀₀₀ bubble lipoplexes and US exposure. (A) OVA presentation on MHC class I molecules in the splenic CD11c⁺ cells at 24 h after transfection by Bare-PEG₂₀₀₀ lipoplexes, Man-PEG₂₀₀₀ lipoplexes, Bare-PEG₂₀₀₀ bubble lipoplexes with US exposure and Man-PEG₂₀₀₀ bubble lipoplexes with US exposure (50 μg pDNA). OVA presentation on MHC class I molecules was determined by IL-2 level secreted from CD8-OVA13 cells co-incubated with the CD11c⁺ cells isolated from once-immunized mice. Each value represents the mean ± SD (n = 4). *p < 0.05; **p < 0.01, compared with the corresponding group of N.T. (B) Schedule of immunization for OVA-specific cytokine secretion experiments and CTL assay. (C) OVA-specific IFN-γ and IL-4 secretion from the splenic cells immunized three times biweekly by Bare-PEG₂₀₀₀ lipoplexes, Man-PEG₂₀₀₀ lipoplexes, Bare-PEG₂₀₀₀ bubble lipoplexes with US exposure and Man-PEG₂₀₀₀ bubble lipoplexes with US exposure (50 μg pDNA). The splenic cells were collected at 2 weeks after last immunization. After the immunized splenic cells were cultured for 72 h in the absence or presence of 100 μg OVA, IFN-γ and IL-4 secreted in the medium were measured by ELISA. Each value represents the mean ± SD (n = 4). **p < 0.01, compared with the corresponding group of OVA. (D) OVA-specific CTL activities after immunization three times by Bare-PEG₂₀₀₀ lipoplexes, Man-PEG₂₀₀₀ lipoplexes, Bare-PEG₂₀₀₀ bubble lipoplexes with US exposure and Man-PEG₂₀₀₀ bubble lipoplexes with US exposure (50 μg pDNA). CTL activities to E.G7-OVA and EL4 cells in the immunized splenic cells were determined by ⁵¹Cr release assay. Each value represents the mean ± SD (n = 4). *p < 0.05; **p < 0.01, compared with the corresponding group of N.T. N.T., non-treatment.

transfection efficiency. In fact, the level of gene expression by this method was higher than that by combination-use method reported previously in the targeted organs (liver and spleen) (Fig. 5) and targeted cells (hepatic NPC and splenic dendritic cells) (Fig. 6); therefore this gene transfection method using Man-PEG₂₀₀₀ bubble lipoplexes and US exposure is more suitable for APC-selective gene transfer *in vivo*.

Since APC-selective and efficient gene expression was observed by transfection using Man-PEG₂₀₀₀ bubble lipoplexes and US exposure, effective therapeutic effects are to be expected by applying this transfection method to DNA vaccine therapy, which the targeted cells are the APCs, using tumor-specific antigen-coding pDNA [31,32]. However, since the level of gene expression by transfection using Man-PEG₂₀₀₀ bubble lipoplexes and US exposure was reduced sequentially (Supplementary Fig. 6), multiple transfections are essential to obtain more effective vaccine effects against cancer (Supplementary Fig. 7). On the other hand, a 2 week interval was needed to achieve the same level of gene expression by

lipoplexes or bubble lipoplexes with US exposure as former transfection in the spleen (Supplementary Fig. 7B and C). Meyer et al. reported that the optimal transfection interval was necessary to achieve high gene expression by the second transfection using lipofection methods because of IFN-γ secretion by intravenous administration of lipoplexes [43]; therefore it is considered that a similar phenomenon is contributed to the sonoporation methods using microbubbles constructed with phospholipids. Based on these findings, we performed the optimization of immunization times (Supplementary Fig. 7) and determined the optimal immunization schedule as shown in Figs. 9B, 10A and 11A.

In DNA vaccine therapy, unlike cancer immunotherapy using tumor-specific antigenic peptides, the peptides expressed as gene products in the cells act as the internal antigen. Since the internal antigens are presented on MHC class I molecules, the strong activation of CTL and high anti-tumor effects are expected in DNA vaccination therapy [44,45]. In this study, by applying this gene transfection method to DNA vaccine therapy using OVA-expressing

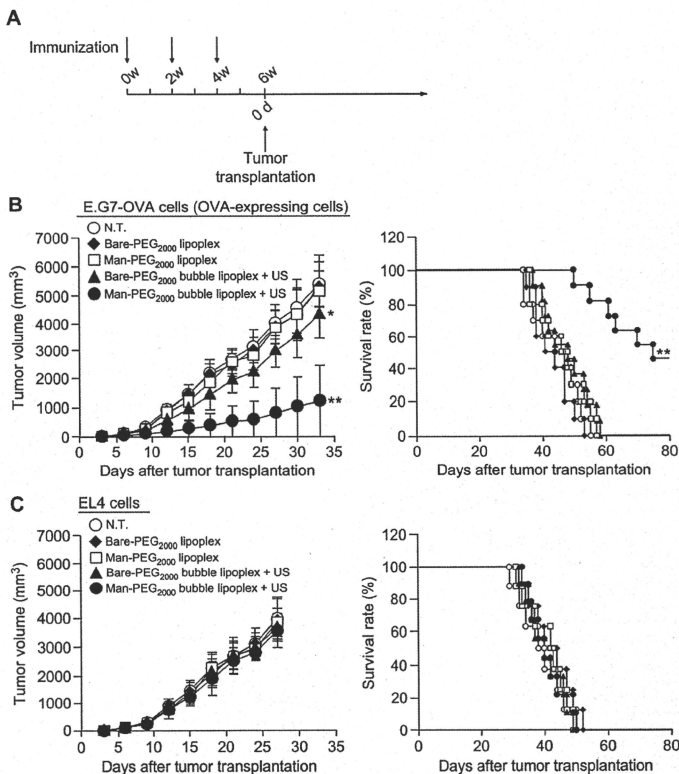


Fig. 10. Anti-tumor effects by DNA vaccination using Man-PEG₂₀₀₀ bubble lipoplexes and US exposure. (A) Schedule of immunization for experiments of therapeutic effects. (B, C) Anti-tumor effects by immunization using Bare-PEG₂₀₀₀ lipoplexes, Man-PEG₂₀₀₀ lipoplexes, Bare-PEG₂₀₀₀ bubble lipoplexes with US exposure and Man-PEG₂₀₀₀ bubble lipoplexes with US exposure (50 µg pDNA). Two weeks after last immunization, (B) E.G7-OVA cells or (C) EL4 cells (1×10^6 cells) were transplanted subcutaneously into the back of mice ($n = 8-11$). The tumor volume was evaluated (each value represents the mean \pm SD) and the survival was monitored up to 80 days after the tumor transplantation. * $p < 0.05$; ** $p < 0.01$, compared with the corresponding group of N.T. N.T., non-treatment.

pDNA, i) the presentation of OVA-peptides on MHC class I molecules of splenic dendritic cells, ii) OVA-specific Th1 cytokine secretion from splenic cells by OVA stimulation and iii) marked activation of CTL against OVA-expressing tumor were observed by gene transfection using Man-PEG₂₀₀₀ bubble lipoplexes constructed with pCMV-OVA and US exposure (Fig. 9). Moreover, high and long-term anti-tumor effects against OVA-expressing tumor were observed in mice transfected by Man-PEG₂₀₀₀ bubble lipoplexes constructed with pCMV-OVA and US exposure (Figs. 10 and 11). It is considered that these results are contributed by APS-selective and efficient gene transfection efficiency using Man-PEG₂₀₀₀ bubble lipoplexes and US exposure. Although more detailed examination by pDNA encoding other tumor-specific antigens, such as gp100 in melanoma or PSA in prostate cancer [45],

is necessary, this transfection method by Man-PEG₂₀₀₀ bubble lipoplexes and US exposure might be available for DNA vaccine therapy.

The gene transfection method using Man-PEG₂₀₀₀ bubble lipoplexes and US exposure was enabled selective and efficient gene transfer to the mannose receptor-expressing cells in the liver such as Kupffer cells and hepatic endothelial cells, which are components of the APCs (Fig. 6A). Therefore, this method is also suitable for anti-inflammatory therapy targeted to Kupffer cells and hepatic endothelial cells, known to play a key role in inflammation [46,47]. In spite of low liver toxicity, since this gene transfection system showed NPC-selective and efficient gene expression in the liver (Fig. 8), better therapeutic effects could be expected by Man-PEG₂₀₀₀ bubble lipoplexes constructed with